

Supporting Information

Transfer of Hydrosulfide from Thiol to Iron(II): A Convenient Synthetic Route for Nonheme Diiron(II)-hydrosulfide Complexes

Nabhendu Pal and Amit Majumdar*

School of Chemical Sciences, Indian Association for the Cultivation of Science, 2A & 2B Raja
S. C. Mullick Road, Kolkata 700032, India.

*Corresponding author email: icam@iacs.res.in

contents	page no.
Experimental Section	S3-S9
Table S1. X-ray crystallographic data for compounds 1a , 1b , 2 and 3 ^a .	S10
Figure S1. (a) Calculation of yield (82%) using Gas Chromatography by comparing area under the curve with externally added standard (mesitylene) and (b) GCMS data for <i>tert</i> -butanol generated during the synthesis of 1a via desulfurization of NaS ^t Bu.	S11
Figure S2. (a) Calculation of yield (26%) using Gas Chromatography by comparing area under the curve with externally added standard (mesitylene) and (b) GCMS data for benzyl alcohol generated during the synthesis of 1a via desulfurization of benzylthiol.	S12
Figure S3. Molecular structure for the cationic part of 2 with 30% probability thermal ellipsoids and partial atom labelling scheme. Hydrogen atoms are omitted for clarity.	S13
Figure S4. IR spectra (solid, KBr pellet) for 1a , 2 , 3 and 4 .	S13
Figure S5. Cyclic voltammetric traces (multiple scans, scan rate = 100 mV/scan) for 1 mM solution of 1a in dichloromethane in the full potential range. Both anodic (a) and cathodic (b) scans are shown.	S14
Figure S6. Cyclic voltammetric traces (multiple scans, scan rate = 100 mV/scan) for 1 mM solution of 2 in dichloromethane. First two redox events (a) and full potential range anodic (b) and cathodic (c) scans are shown.	S15
Figure S7. Cyclic voltammetric traces (multiple scans, scan rate = 100 mV/scan) for 1 mM solution of 3 in dichloromethane in the full potential range. Both anodic (a) and cathodic (b) scans are shown.	S16
Figure S8. Absorption spectroscopic signatures for 1a and 3 in DMF ([1a] = [3] = 2 × 10 ⁻⁴ M).	S16
Figure S9. Absorption spectroscopic signatures for 2 and 4 in DMF ([2] = [4] = 2 × 10 ⁻⁴ M).	S17
Figure S10. NIR spectroscopic signatures for 1a , 3 and 4 in DMF ([1a] = [3] = [4] = 2 mM).	S17
Figure S11. Absorption spectroscopic signatures for 3 and 4 as solid samples.	S18
Figure S12. Mass spectrometric data for 1a in MeCN. m/z calculated for [Fe ₂ (<i>N</i> -Et-HPTB)(SH)(H ₂ O)(MeCN)] ²⁺ = 463.655 (simulated, green line), m/z observed = 463.123 (red line).	S18
Figure S13. Mass spectrometric data for 2 in MeCN. m/z calculated for [Fe ₂ (<i>N</i> -Et-HPTB)(Cl)(DMF) ₂] ²⁺ = 435.131 (simulated, red line), m/z observed = 434.552 (green line).	S19
Figure S14. Mass spectrometric data for 3 in MeCN. m/z calculated for [Fe ₂ (<i>N</i> -Et-HPTB)(SH)(H ₂ O)(DMF) ₂] ³⁺ = 344.466 (simulated, green line), m/z observed = 344.964 (red line).	S19
Figure S15. Mass spectrometric data for 4 in MeCN. m/z calculated for [Fe ₂ (<i>N</i> -Et-HPTB)(Cl)(H ₂ O)(DMF) ₂] ³⁺ = 345.129 (simulated, green line), m/z observed = 345.154 (red line).	S20
Figure S16. X-ray photoelectron spectroscopic data showing binding energy for the sulfur 2p levels of (a) 1a and (b) 3 .	S20
Figure S17. X-ray photoelectron spectroscopic data showing binding energy for the (a) Fe 2p levels and (b) chlorine 2p levels of 2 .	S21
Figure S18. Full range plot of the X-ray photoelectron spectroscopic data for (a) 1a and (b) 2 .	S21
Figure S19. X-ray photoelectron spectroscopic data showing binding energy for the (a) Fe 2p levels and (b) chlorine 2p levels of 4 .	S22
Figure S20. Full range plot of the X-ray photoelectron spectroscopic data for (a) 3 and (b) 4 .	S22
Figure S21. Kinetic plots for the initial rate of formation of (a) 1a ·O ₂ and (b) 2 ·O ₂ at -80°C.	S23
Figure S22. Absorption spectroscopic monitoring for the decomposition of (a) 1a ·O ₂ and (b) 2 ·O ₂ at RT. [1a] = 0.75 mM in CH ₂ Cl ₂ :DMSO (10:1), O ₂ purged for 30 seconds, scan rate = 15 seconds/scan, total time = 120 minutes. [2] = 0.5 mM in CH ₂ Cl ₂ :DMSO (10:1), O ₂ purged for 10 seconds, scan rate = 15 seconds/scan, total time = 110 minutes.	S23
Figure S23. Kinetic plots (decomposition traces and half life calculations) for the decomposition of (a) 1a ·O ₂ (t _{1/2} = 15.4 minutes) and (b) 2 ·O ₂ (t _{1/2} = 22.8 minutes) at RT. Decomposition product in each case was characterized as [Fe ₄ (<i>N</i> -Et-HPTB) ₂ (μ-O) ₃ (H ₂ O) ₂](BF ₄) ₂ . ⁴	S24
Figure S24. ³¹ P NMR spectrum for the product obtained after reaction of 1a ·O ₂ with PPh ₃ at RT showing the presence of Ph ₃ PS (δ = 43.34 ppm) along with Ph ₃ PO (δ = 29.32 ppm) and unreacted PPh ₃ (δ = -5.39 ppm).	S25
Figure S25. ³¹ P NMR spectrum for the product obtained after reaction of 1a ·O ₂ with PPh ₃ at -40°C showing the presence of only PPh ₃ (δ = -5.39 ppm).	S26
Figure S26. ³¹ P NMR spectrum for the product obtained after stirring elemental sulfur (S ₈) in toluene at -40°C overnight, followed by filtration, evaporation of the filtrate and reaction of the residue with PPh ₃ in CDCl ₃ at RT, showing the presence of PPh ₃ (δ = -5.41 ppm) and Ph ₃ PS (δ = 43.17 ppm).	S27
Figure S27. GC traces for (a) elemental sulfur (S ₈ , 0.1 mM in CCl ₄) and (b) elemental sulfur produced upon decomposition of 1a ·O ₂ at RT. Also shown is the GCMS data for the elemental sulfur produced upon decomposition of 1a ·O ₂ at RT (c).	S28
Figure S28. ¹ H NMR of 1a in CD ₃ CN.	S29
Figure S29. ¹ H NMR of 2 in CD ₃ CN.	S29
Figure S30. ¹ H NMR of 3 in CD ₃ CN.	S30
Figure S31. ¹ H NMR of 4 in CD ₃ CN.	S30
References	S31

Experimental Section

Preparation of Compounds. All reactions and manipulations were performed under a pure argon atmosphere using either standard Schlenk techniques or an inert atmosphere box. Solvents were dried following standard procedures.¹ HN-Et-HPTB² was synthesized following a reported procedure.³ All the chemicals were obtained from commercial sources and were used without further purification. All the filtrations were performed through Celite and solvent removal steps were carried out in vacuo inside an inert atmosphere glove box under dinitrogen atmosphere. Yields reported for iron complexes in each case are for recrystallized compounds, calculated using corresponding molecular weights of the compounds shown in table S1 with the consideration that one equivalent of ligand will produce one equivalent of the dinuclear complexes.

*[Fe₂(N-Et-HPTB)(SH)(H₂O)](BF₄)₂·DMF (**1a**).* To a mixture of H-N-Et-HPTB (0.08 mmol, 57.8 mg), Et₃N (0.12 mmol, 12.1 mg) and NaS^tBu (0.12 mmol, 15 mg) in 2 mL of DMF was added Fe(BF₄)₂·6H₂O (0.16 mmol, 54.5 mg) with stirring and the resultant slurry was stirred for 6h. The reaction mixture was filtered. Et₂O was allowed to diffuse into the pale yellow filtrate overnight at -35°C with additional standing for 1 day at RT to afford **1a** as a colorless crystalline solid (68 mg, 75%). Under identical reaction conditions, use of ^tBuSH and PhCH₂SH instead of NaS^tBu afforded **1a** in 71% (77 mg) and 33% (30 mg) yields respectively. IR (KBr pellet): $\nu_{\text{SH}} = 2515 \text{ cm}^{-1}$. ESI-MS (in MeCN): $m/z = 463.12$ (calculated m/z from simulation = 463.65) for $[\text{Fe}_2(\text{N-Et-HPTB})(\text{SH})(\text{H}_2\text{O})(\text{MeCN})]^{2+}$. XPS: Binding energy = 162.25 eV (S 2P), 709.85 eV (Fe 2P_{3/2} level), 722.97 eV (Fe 2P_{1/2} level), 714.60 eV (satellite peak).

In an alternate method, NaS^tBu (0.06 mmol, 7.2mg) was added with stirring to a solution of $[\text{Fe}_2(\text{N-Et-HPTB})(\text{DMF})_4](\text{BF}_4)_3^{2,4}$ (0.04mmol, 55.5 mg) and Et₃N (0.06 mmol, 6.4 mg) in 2 mL of DMF. The reaction mixture was stirred for 4h and filtered. Et₂O was allowed to diffuse into

the pale yellow filtrate overnight at -35°C with additional standing for 1 day at RT to afford **1a** as a colorless crystalline solid (30 mg, 62%).

In some cases, $[\text{Fe}_2(\text{N-Et-HPTB})(\text{SH})(\text{DMF})_2](\text{BF}_4)_2 \cdot 2\text{DMF}$ (**1b**) was isolated during the synthesis of **1a**. It may be noted that **1a** and **1b** essentially represent the same compound except for the nature of the coordinating solvents. Reasonable elemental analysis could not be obtained for **1a**, possibly due to the formation of **1b** along with **1a** during the synthesis of **1a**.

$[\text{Fe}_2(\text{N-Et-HPTB})(\text{Cl})(\text{DMF})_2](\text{BF}_4)_2 \cdot 2\text{DMF}$ (**2**). To a mixture of H-N-Et-HPTB (0.08 mmol, 57.8 mg), Et_3N (0.12 mmol, 12.1 mg) and $(\text{Bu}_4\text{N})(\text{Cl})$ (0.12 mmol, 33.5 mg) in 2 mL of DMF was added $\text{Fe}(\text{BF}_4)_2 \cdot 6\text{H}_2\text{O}$ (0.16 mmol, 54.5 mg) with stirring and the resultant slurry was stirred for 6h. The reaction mixture was filtered. Et_2O was allowed to diffuse into the colorless filtrate overnight at -35°C with additional standing for 1 day at RT to afford the product as a colorless crystalline solid (68 mg, 64%). Anal Calcd for $\text{C}_{55}\text{H}_{77}\text{B}_2\text{ClF}_8\text{Fe}_2\text{N}_{14}\text{O}_5 \cdot 1\text{H}_2\text{O}$ (**2**· H_2O): C, 48.82%; H, 5.88%; N, 14.49%. Found C, 49.02%; H, 5.88%; N, 14.67%. ESI-MS: $m/z = 434.552$ (calculated m/z from simulation = 435.131) for $[\text{Fe}_2(\text{N-Et-HPTB})(\text{Cl})(\text{DMF})_2]^{2+}$.

$[\text{Fe}_2(\text{N-Et-HPTB})(\text{SH})(\text{H}_2\text{O})(\text{DMF})_2](\text{BF}_4)_3$ (**3**). A solution of $(\text{Cp}_2\text{Fe})(\text{BF}_4)$ (0.075mmol, 20.4 mg) in 1 mL of MeCN was added dropwise into a solution of **1a** (0.05mmol, 72mg) in 1 mL of MeCN with stirring. The stirring was continued for 2 h, after which the solvent was evaporated to dryness. The solid residue was washed thoroughly with THF and the residue was then dissolved in 1 mL of DMF and filtered through Celite. Et_2O was allowed to diffuse into the red colored filtrate overnight at -35°C with additional standing for 1 day at RT to afford the product as red colored crystalline solid (52 mg, 81%). Anal Calcd for $\text{C}_{49}\text{H}_{65}\text{B}_3\text{F}_{12}\text{Fe}_2\text{N}_{12}\text{O}_4\text{S}_1 \cdot \text{C}_3\text{H}_7\text{NO}$ (**3**· $\text{C}_3\text{H}_7\text{NO}$): C, 45.81%; H, 5.32%; N, 13.36%. Found C, 45.80%; H, 5.19; N, 13.52%. IR (KBr

pellet): $\nu_{\text{SH}} = 2515 \text{ cm}^{-1}$. ESI-MS: $m/z = 344.455$ (calculated m/z from simulation = 344.466) for $[\text{Fe}_2(\text{N-Et-HPTB})(\text{SH})(\text{H}_2\text{O})(\text{DMF})_2]^{3+}$. Solution magnetic moment (μ_{eff}) for three different batches of **3**: 1.793 BM, 1.800 BM, 1.780 BM (theoretical $\mu_{\text{eff}} = 1.732$ for $S = \frac{1}{2}$ system). UV-Vis-NIR: $\lambda_{\text{max}} = 1430 \text{ nm}$, $\epsilon = 310 (\pm 30) \text{ M}^{-1} \text{ cm}^{-1}$ (inter-valence charge transfer). XPS: Binding energy = 162.72 eV (S 2P); 709.41 eV and 711.56 eV (Fe 2P_{3/2}); 722.25 eV (Fe 2P_{1/2}); 714.75 eV and 718.50 eV (satellite peaks).

$[\text{Fe}_2(\text{N-Et-HPTB})(\text{Cl})(\text{H}_2\text{O})(\text{DMF})_2](\text{BF}_4)_3$ (**4**). A solution of $(\text{Cp}_2\text{Fe})(\text{BF}_4)$ (0.075 mmol, 20.4 mg) in 1 mL of MeCN was added dropwise into a solution of **2** (0.05 mmol, 67 mg) in 1 mL of MeCN with stirring. The stirring was continued for 2 h, after which the solvent was evaporated to dryness. The solid residue was washed thoroughly with THF and the residue was then dissolved in 1 mL of DMF and filtered through Celite. Et₂O was allowed to diffuse into the red colored filtrate overnight at -35°C with additional standing for 1 day at RT to afford the product as red colored crystalline solid (52 mg, 80%). Anal Calcd for $\text{C}_{49}\text{H}_{65}\text{B}_3\text{ClF}_{12}\text{Fe}_2\text{N}_{12}\text{O}_4$ (**4**): C, 45.49%; H, 5.06%; N, 12.99%. Found C, 45.01%; H, 4.73%; N, 13.12%. ESI-MS: $m/z = 345.153$ (calculated m/z from simulation = 345.129) for $[\text{Fe}_2(\text{N-Et-HPTB})(\text{Cl})(\text{H}_2\text{O})(\text{DMF})_2]^{3+}$. Solution magnetic moment (μ_{eff}) for three different batches of **4**: = 1.818 BM, 1.798 BM and 1.817 BM (theoretical $\mu_{\text{eff}} = 1.732$ for $S = \frac{1}{2}$ system). UV-Vis-NIR: $\lambda_{\text{max}} = 1430 \text{ nm}$, $\epsilon = 190 (\pm 5) \text{ M}^{-1} \text{ cm}^{-1}$ (inter-valence charge transfer). XPS: Binding energy = 196.81 eV (Cl 2P_{3/2}), 198.34 eV (Cl 2P_{1/2}); 709.34 eV and 711.72 eV (Fe 2P_{3/2}); 722.86 (Fe 2P_{1/2}); 715.25 eV and 718.08 eV (satellite peaks).

General Physical Methods. Elemental analysis was recorded using a Perkin-Elmer 2400 series II CHNS analyzer. Electronic absorption spectra of the complexes were recorded using a Cary 60 UV-Vis spectrophotometer. High resolution mass spectra were recorded using Q-Tof-micro MS

system using electron spray ionization (ESI) techniques. Electrochemical studies of the complexes (10^{-3} M in MeCN) were performed using a CHI620E electrochemical analyzer (CH Instruments, USA). A three electrode setup was employed, consisting of a glassy carbon working electrode, a platinum wire auxiliary electrode, and a silver wire (as the pseudo-reference electrode). Tetra-n-butylammonium hexafluorophosphate (0.1 M) was used as the supporting electrolyte. Electrochemical potentials are referenced internally to the ferrocene/ferrocenium couple at 0.0 V. Fourier transform infrared spectroscopy on KBr pellets was performed on a Shimadzu FT-IR 8400S instrument. Solution electronic spectra (single and time-dependent) for the oxygenation study of diiron complexes were measured on an Agilent 8453 diode array spectrophotometer. UV-vis-NIR absorption spectra were recorded on a Perkin-Elmer Lambda 950 UV/vis spectrophotometer and a J&M TIDAS instrument. ^{31}P NMR and ^1H NMR spectra were taken on a Bruker Avance DPX 300/400 MHz spectrometer. XPS analysis of the complexes was carried out by using a X-ray photoelectron spectroscopic (XPS, Omicron, model:1712-62-11) method. Measurement was done by using an Al- K_{α} radiation source under 15kV voltages and 5 mA current.

Gas Chromatographic Methods. GC-MS measurements were carried out either with a Thermo Scientific Trace 1310 gas chromatograph coupled with a ISQ QD Mass spectrometer with a maximum temperature 300°C using a TG-5MS (30m x 0.25mm x 0.25 μm) column or a Perkin-Elmer Clarus 600 using an Elite 5 MS (30 m x 0.25 mm x 0.25 μm) column with a maximum temperature of 300°C . The samples for the GC experiments were prepared from the crude reaction mixture containing $[\text{Fe}_2(\text{N-Et-HPTB})(\text{DMF})_4](\text{BF}_4)_3$, thiols/sodium salt of thiolate, Et_3N in DMF obtained after isolating the crystals of **1a/1b** by addition of Et_2O and thereby making the solution metal free. To this crude reaction solution (DMF/ Et_2O), 0.05 mmol of mesitylene

(external standard) was added since 0.05 mmol of $[\text{Fe}_2(\text{N-Et-HPTB})(\text{DMF})_4](\text{BF}_4)_3$ was used during the synthesis of **1a/1b** with different thiols. From this homogeneous solution 1.0 μL was injected in GCMS for analysis. Yield of the organic product = Response factor \times 100% = (Area under the curve of organic product) / (Area under the curve of mesitylene) \times 100%.

^{31}P NMR Spectroscopic Measurements.

Oxygen was purged for 30 seconds into a solution of 55 mg (0.05mmol) of **1a** in 3 ml MeCN at -40°C to generate a blue colored solution (characteristic of **1a** $\cdot\text{O}_2$). The blue solution was then allowed to warm up to RT and kept standing for overnight. The solution was then evaporated to dryness. A solution of PPh_3 (0.1 mmol, 26.2 mg) in 1 ml CDCl_3 was added into the residue and the mixture was stirred overnight under inert atmosphere. The reaction mixture was filtered through celite and ^{31}P NMR spectrum of the filtrate was recorded (figure S24).

In another experiment, oxygen was purged for 30 seconds into a solution of 55 mg (0.05mmol) of **1a** in 3 ml MeCN at -40°C to generate a blue colored solution (characteristic of **1a** $\cdot\text{O}_2$). Pre-cooled Et_2O was added into the solution maintained at -40°C to immediately precipitate **1a** $\cdot\text{O}_2$. After 10 minutes, 2 mL of pre-cooled toluene was added into the solution and the mixture was stirred overnight at -40°C . The reaction mixture was then filtered and the filtrate was evaporated. A solution of PPh_3 (0.1 mmol, 26.2 mg) in 1 ml CDCl_3 was added into the residue and the mixture was stirred overnight at RT under inert atmosphere. The reaction mixture was filtered through celite and ^{31}P NMR spectrum of the filtrate was recorded (figure S25).

In a blank experiment, 1.6 mg (0.05 mmol) of elemental sulfur (S_8) was stirred overnight in 2 mL of toluene at -40°C . The reaction mixture was then filtered and the filtrate was evaporated. A solution of PPh_3 (0.1 mmol, 26.2 mg) in 1 ml CDCl_3 was added into the residue and the mixture

was stirred overnight at RT under inert atmosphere. The reaction mixture was filtered through celite and ^{31}P NMR spectrum of the filtrate was recorded (figure S26).

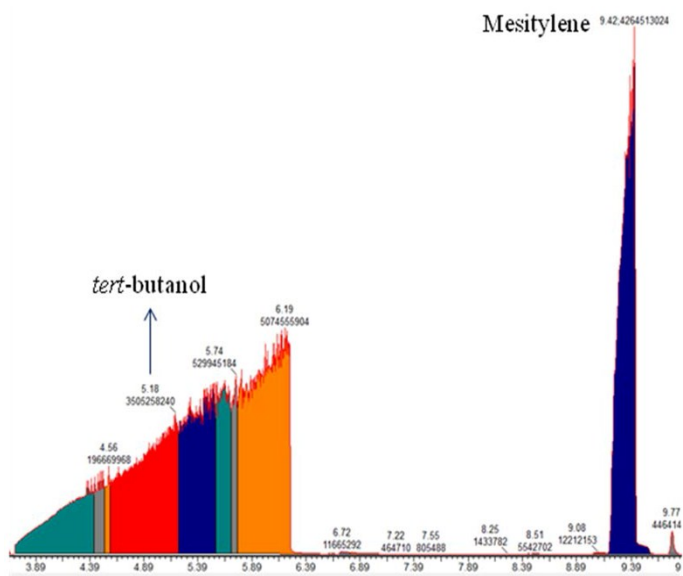
X-ray Structure Determinations. The molecular structures of the 4 compounds **1a**, **1b**, **2** and **3** were determined by single crystal X-ray structure determinations. It may be noted that the final R values for two X-ray structures (**1a** and **2**) are higher than 10%. Despite of attempted crystallization from different solvent combinations, we could not get better crystals for these complexes. Also, it may be possible that there is a S/O disorder in the X-ray structures of **1a** and **3**, which could not be modeled due to unavailability of good data set. Nevertheless, in addition to single crystal X-ray structure determination, identity and bulk purity for **1a**, **1b**, **2** and **3** were determined by a combination of elemental analysis, ESI-MS, cyclic voltammetry, IR spectroscopy, UV-Vis and UV-Vis NIR spectroscopy, solution magnetic measurements by Evans method and X-ray photoelectron spectroscopy. Diffraction-quality crystals were obtained as described in the syntheses of the respective compounds. Single crystals were coated with Parabar oil and were mounted under 100 K nitrogen cold stream. Data collections were performed either on a Bruker SMART APEX-II diffractometer with graphite-monochromated Mo $K\alpha$ radiation ($\lambda = 0.71073 \text{ \AA}$) controlled by the APEX II (v. 2010.1-2) software package (**1b**) or by using a Bruker D8 VENTURE Microfocus diffractometer equipped with PHOTON II Detector, with Mo $K\alpha$ radiation ($\lambda = 0.71073 \text{ \AA}$), controlled by the APEX III (v2017.3-0) software package (**1a**, **2** and **3**). The raw data were integrated and corrected for Lorentz and polarization effects with the aid of the Bruker APEX II/APEX III program suite.⁵ Absorption corrections were performed by using SADABS. Space groups were assigned by systematic absences (determined by XPREP) and analysis of metric symmetry and were further checked in each case by PLATON^{6,7} for additional symmetry. Structures were solved by direct methods and refined against all data in the

reported 2 θ ranges by full-matrix least squares on F² using the SHELXL program suite⁸ in the OLEX 2⁹ interface. Hydrogen atoms at idealized positions were included in final refinements. The OLEX 2 interface was used for structure visualization as well as for drawing ORTEP^{10,11} plots. Complexes **1b** and **3** contain severely disordered solvent molecules (DMF) which were treated using MASK procedure in OLEX2 (equivalent to SQUEEZE in PLATON). Details of the MASK procedure and results are provided in the respective cifs. Crystallographic data and final agreement factors are provided in table 1. Further details on the crystal structure investigation(s) may be obtained from the Cambridge Crystallographic Data Centre (CCDC) using www.ccdc.cam.ac.uk/deposit. CCDC 1871395-1871398 contain the supplementary crystallographic data for this paper. These data are provided free of charge by The Cambridge Crystallographic Data Centre.

Table S1. X-ray crystallographic data for compounds **1a**, **1b**, **2** and **3**^a.

compounds	1a	1b	2	3
CCDC entry	1871397	1871396	1871398	1871395
temperature (K)	100(2)	100(2)	100(2)	100(2)
formula	C ₄₆ H ₅₉ B ₂ F ₈ Fe ₂ N ₁₁ O ₃ S	C ₅₅ H ₇₈ B ₂ F ₈ Fe ₂ N ₁₄ O ₅ S	C ₅₅ H ₇₇ B ₂ ClF ₈ Fe ₂ N ₁₄ O ₅	C ₄₉ H ₆₆ B ₃ F ₁₂ Fe ₂ N ₁₂ O ₄ S
formula weight	1131.42	1332.69	1335.07	1291.32
crystal system	monoclinic	triclinic	triclinic	triclinic
space group	P2 ₁ /n	P-1	P-1	P-1
a, Å	13.9837(16)	12.226(2)	12.253(3)	13.584(4)
b, Å	22.878(3)	15.384(3)	15.368(4)	14.829(4)
c, Å	16.0002(16)	18.398(3)	18.420(5)	19.058(5)
α, deg	90	102.922(5)	102.748(8)	67.164(9)
β, deg	97.816(3)	96.739(5)	96.655(7)	72.810(9)
γ, deg	90	98.616(6)	98.924(7)	76.576(9)
V, Å ³	5071.2(10)	3293.5(10)	3301.6(14)	3349.9(17)
Z	4	2	2	2
ρ _{calcd} , gm/cm ³	1.482	1.344	1.343	1.280
μ, mm ⁻¹	0.695	0.550	0.557	0.544
θ range, deg	2.196-25.746	2.300-25.619	2.197-25.834	2.340-25.837
completeness to θ, %	99.6	97.1	97.5	98.4
reflections collected	129203	26542	30663	32546
independent reflections	9652	12066	12419	12753
R(int)	0.1543	0.0653	0.0961	0.0827
restraints ^b	93	42	7	142
parameters	568	776	772	674
Max., min. transmission	0.7453, 0.6561	0.7452, 0.4597	0.7453, 0.4962	0.7453, 0.5899
R1 ^c (wR2) ^d [I>2σ(I)]	0.1418 (0.4088)	0.0918 (0.2053)	0.1013 (0.2707)	0.0913 (0.2535)
R1 ^c (wR2) ^d	0.2097 (0.4539)	0.1296 (0.2338)	0.1737 (0.3187)	0.1189 (0.2793)
GOF(F2) ^e	1.613	1.032	1.032	1.074
^f max, min peaks, e.Å ³	1.732, -1.212	1.081, -0.728	0.868, -0.696	1.379, -1.212

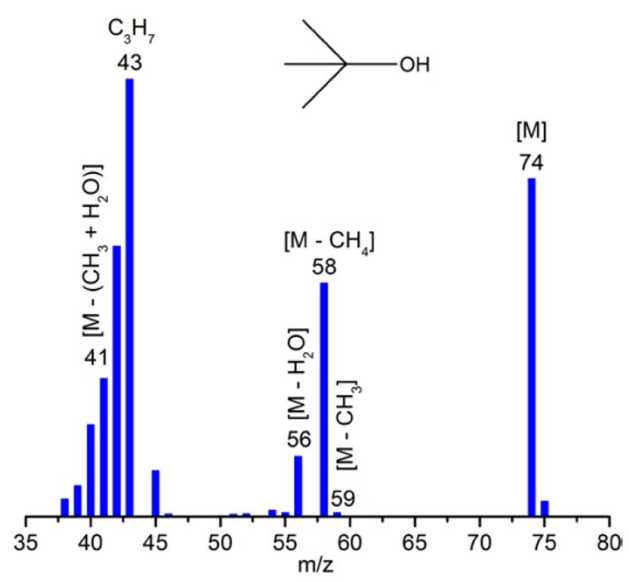
^aMo Kα radiation (λ = 0.71073 Å). ^b**1a**, disordered BF₄⁻, DMF and ligand; **1b**, disordered BF₄⁻ and DMF; **2**, disordered BF₄⁻ and DMF; **3**, disordered BF₄⁻, DMF and ligand. ^cR1 = Σ||Fo|-|Fc||/Σ|Fo|. ^dwR2 = {Σ[w(Fo2-Fc2)2]/Σ[w(Fo2)2]}^{1/2}. ^eGOF = {Σ[w(Fo2-Fc2)2]/(n-p)}^{1/2}, where n is the number of data and p is the number of refined parameters. ^felectron density near: **1a**, -SH; **1b**, -SH; **2**, Fe2; **3**, O2 (terminal water).



Retention Time	Peak Area
5.18	3505258240
9.42	4264513024

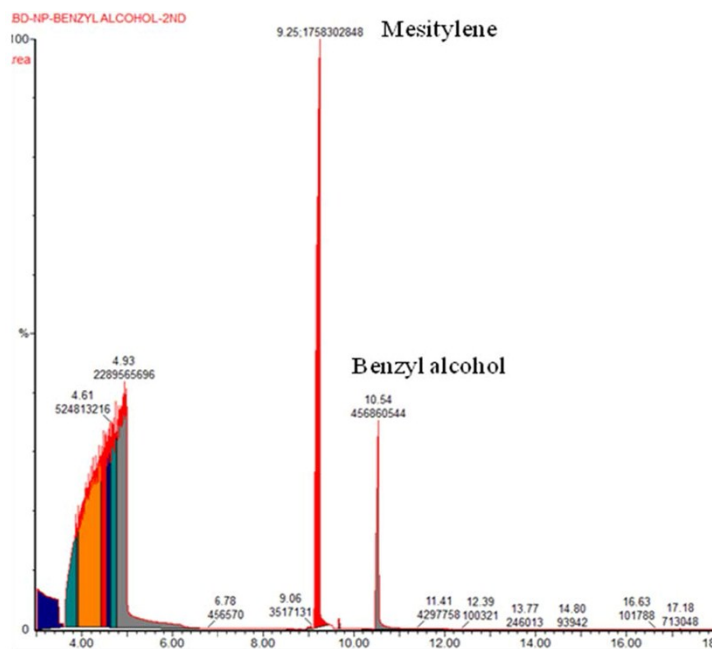
$$\text{Yield} = \frac{3505258240}{4264513024} \times 100\% = 82.2\%$$

(a)



(b)

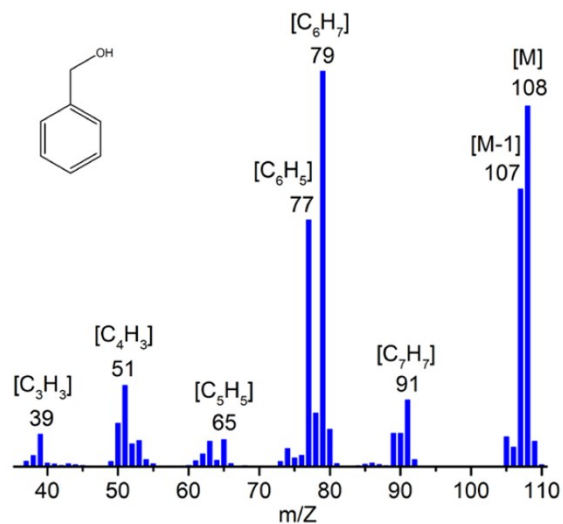
Figure S1. (a) Calculation of yield (82%) using Gas Chromatography by comparing area under the curve with externally added standard (mesitylene) and (b) GCMS data for *tert*-butanol generated during the synthesis of **1a** via desulfurization of NaS'Bu.



Retention Time	Peak Area
10.64	456860544
9.25	1758302848

$$\text{Yield} = \frac{456860544}{1758302848} \times 100\% = 25.98\%$$

(a)



(b)

Figure S2. (a) Calculation of yield (26%) using Gas Chromatography by comparing area under the curve with externally added standard (mesitylene) and (b) GCMS data for benzyl alcohol generated during the synthesis of **1a** via desulfurization of benzylthiol.

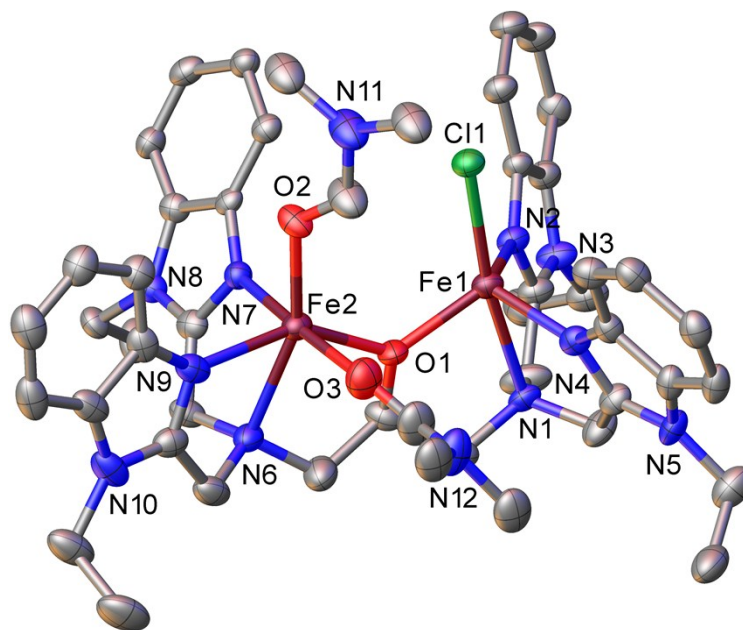


Figure S3. Molecular structure for the cationic part of **2** with 30% probability thermal ellipsoids and partial atom labelling scheme. Hydrogen atoms are omitted for clarity.

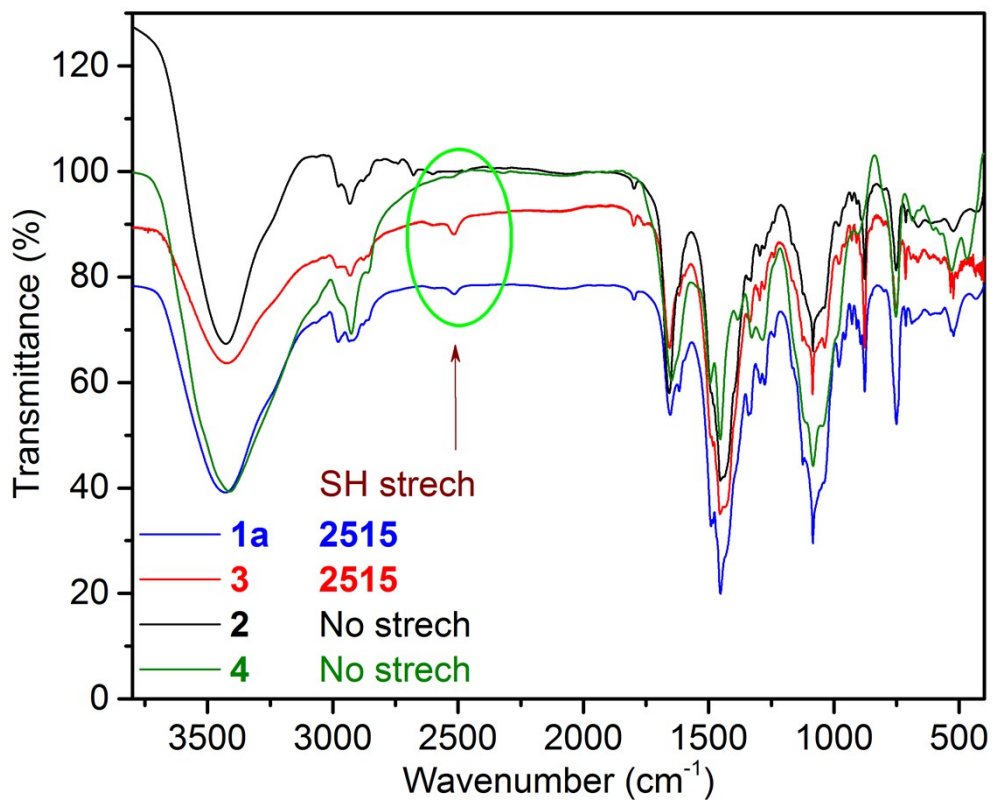


Figure S4. IR spectra (solid, KBr pellet) for **1a**, **2**, **3** and **4**.

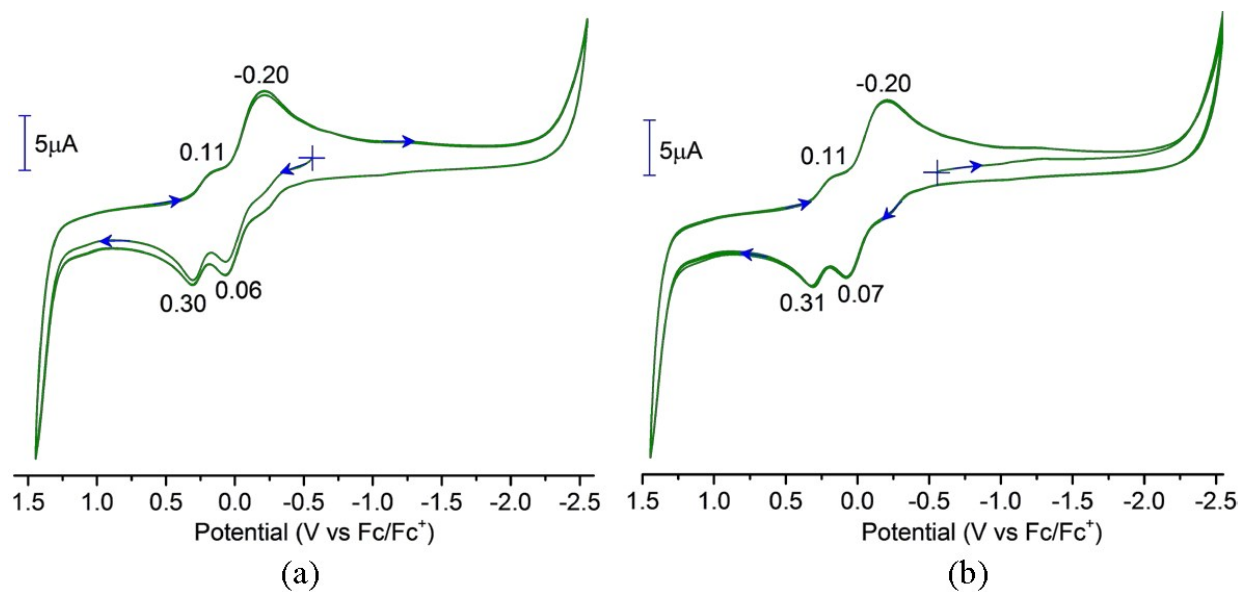


Figure S5. Cyclic voltammetric traces (multiple scans, scan rate = 100 mV/scan) for 1 mM solution of **1a** in dichloromethane in the full potential range. Both anodic (a) and cathodic (b) scans are shown.

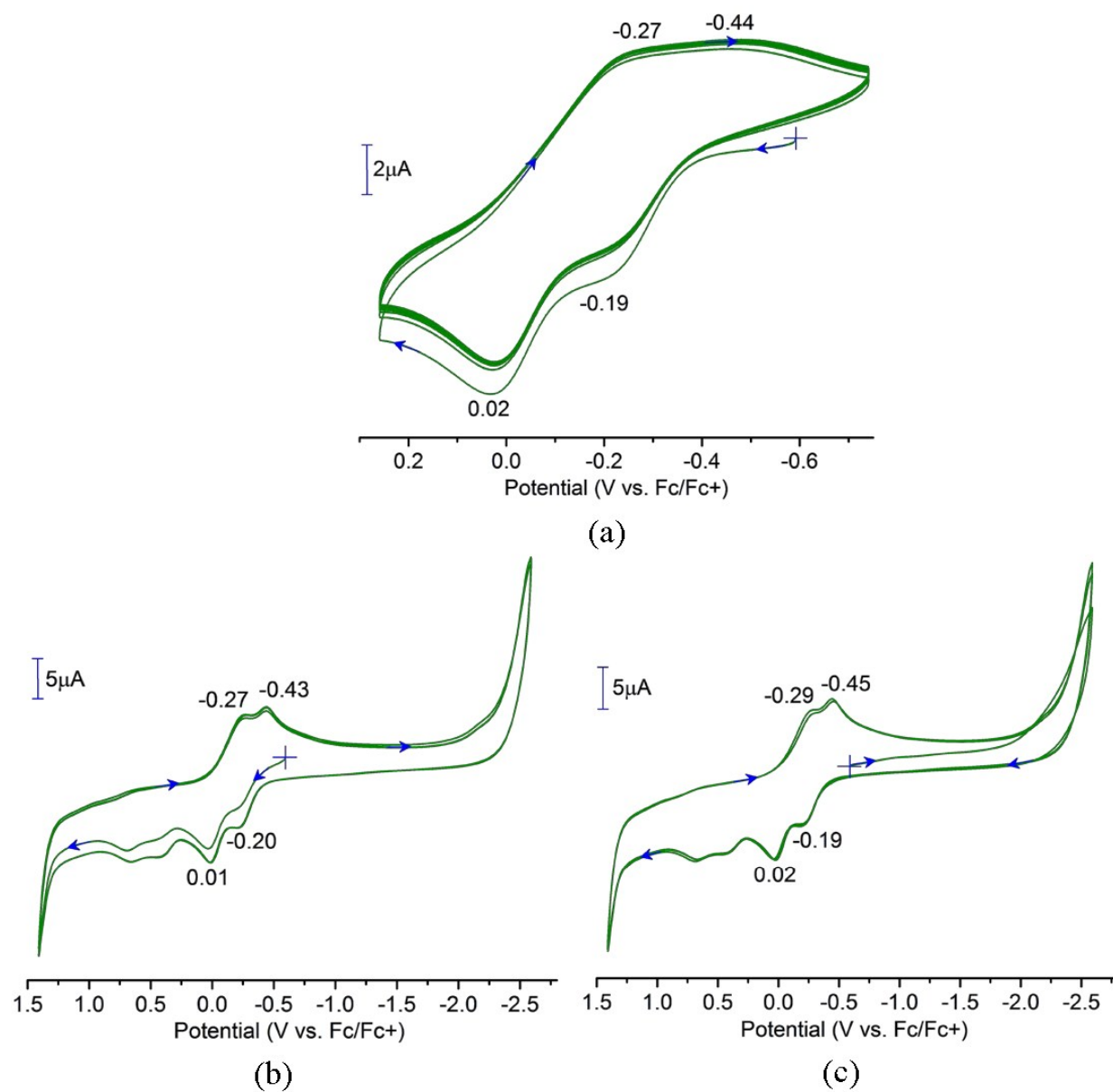


Figure S6. Cyclic voltammetric traces (multiple scans, scan rate = 100 mV/scan) for 1 mM solution of **2** in dichloromethane. First two redox events (a) and full potential range anodic (b) and cathodic (c) scans are shown.

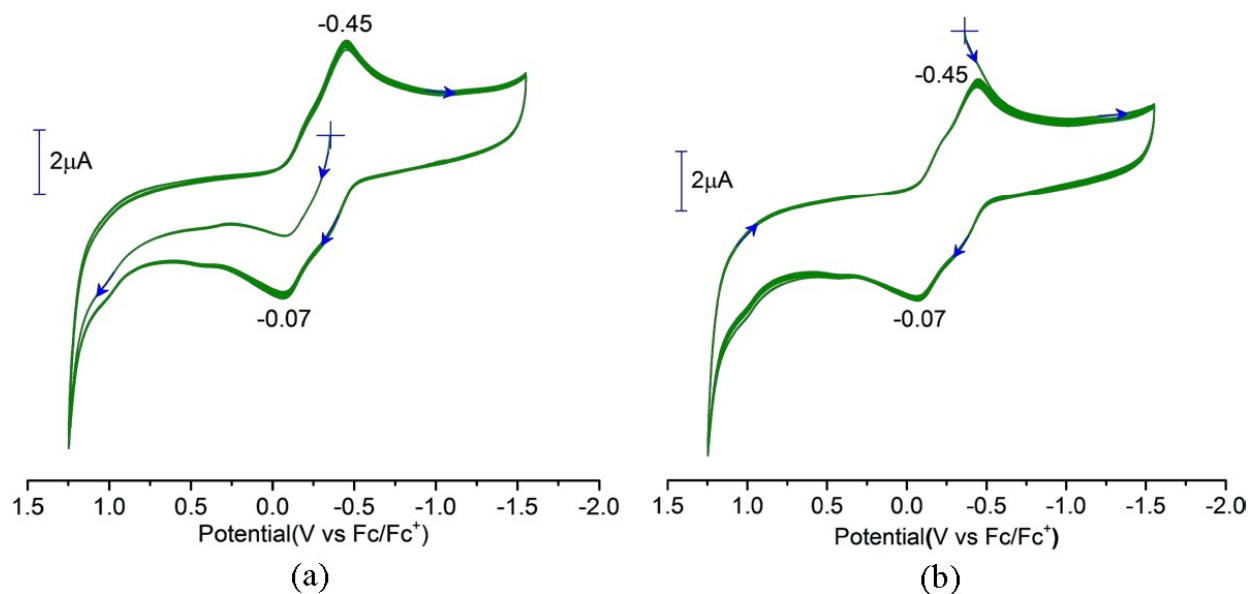


Figure S7. Cyclic voltammetric traces (multiple scans, scan rate = 100 mV/scan) for 1 mM solution of **3** in dichloromethane in the full potential range. Both anodic (a) and cathodic (b) scans are shown.

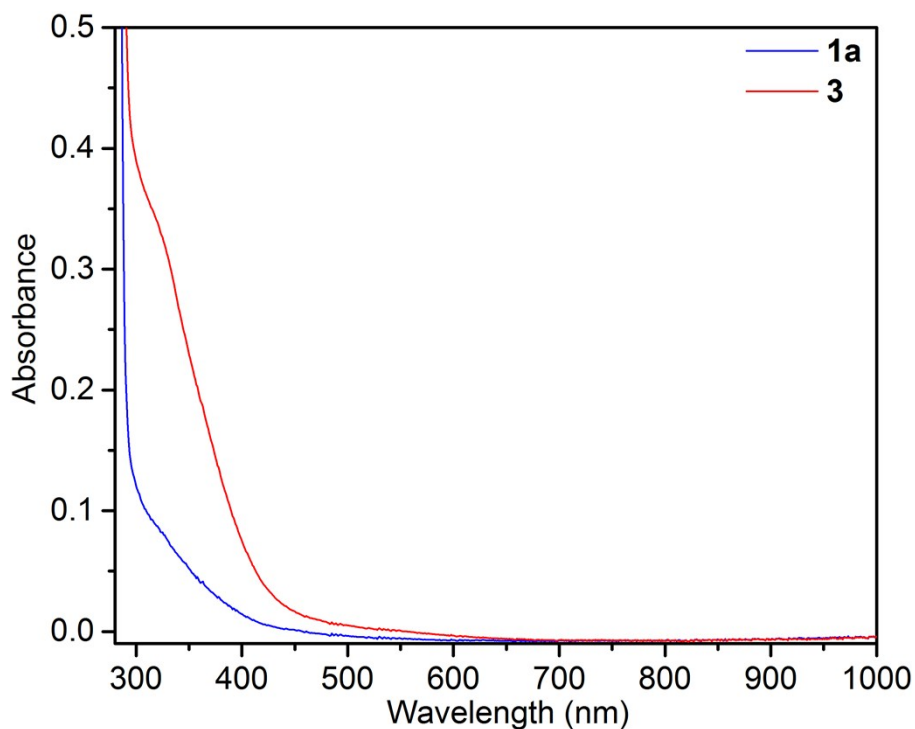


Figure S8. Absorption spectroscopic signatures for **1a** and **3** in DMF ($[\mathbf{1a}] = [\mathbf{3}] = 2 \times 10^{-4}$ M).

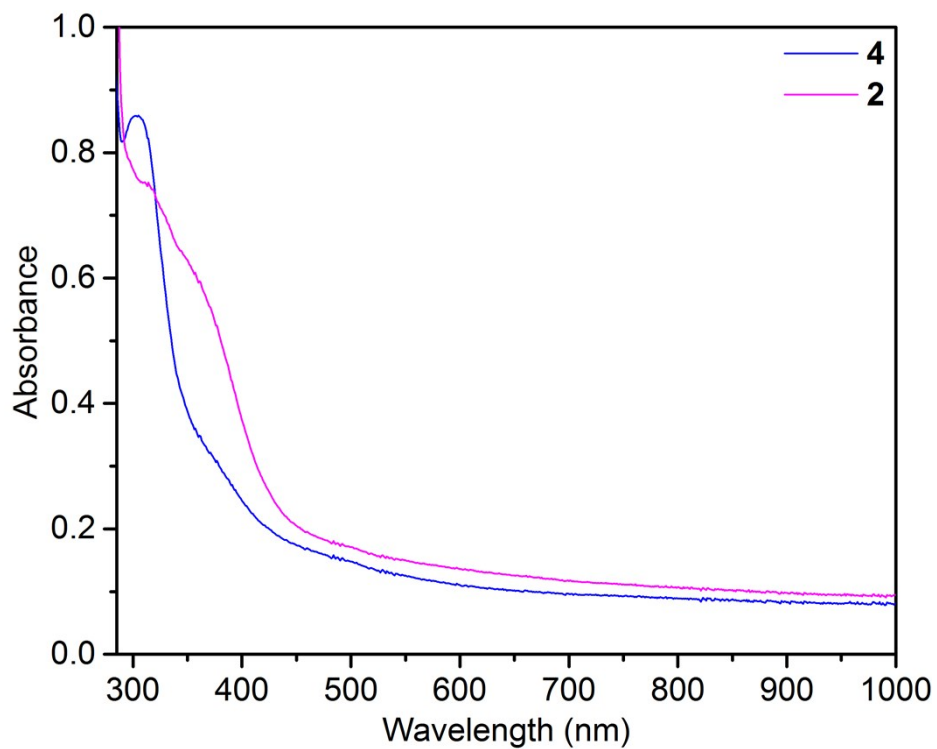


Figure S9. Absorption spectroscopic signatures for **2** and **4** in DMF ($[2] = [4] = 2 \times 10^{-4}$ M).

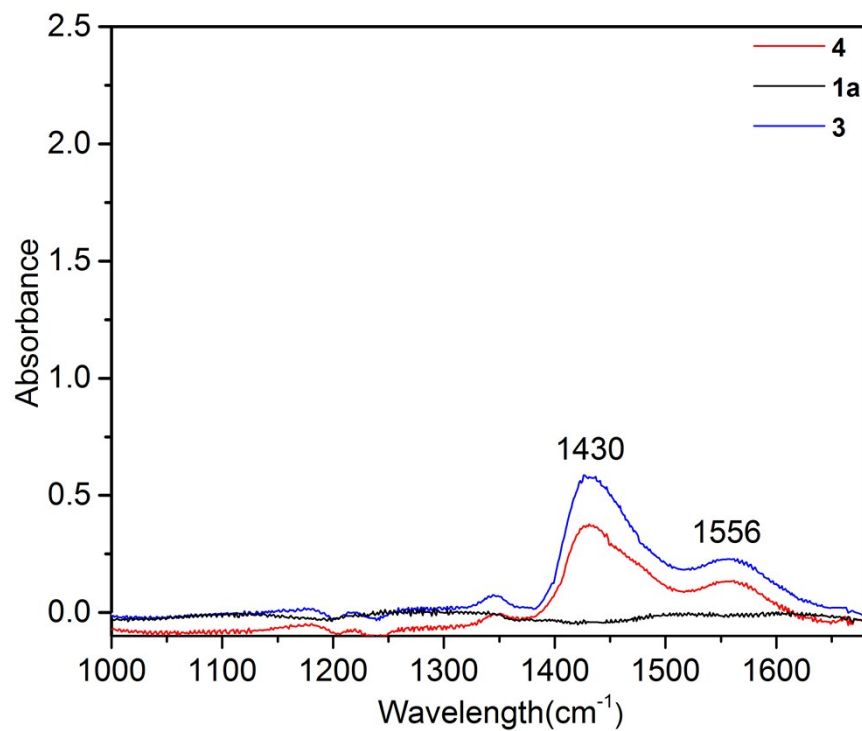


Figure S10. NIR spectroscopic signatures for **1a**, **3** and **4** in DMF ($[1a] = [3] = [4] = 2$ mM).

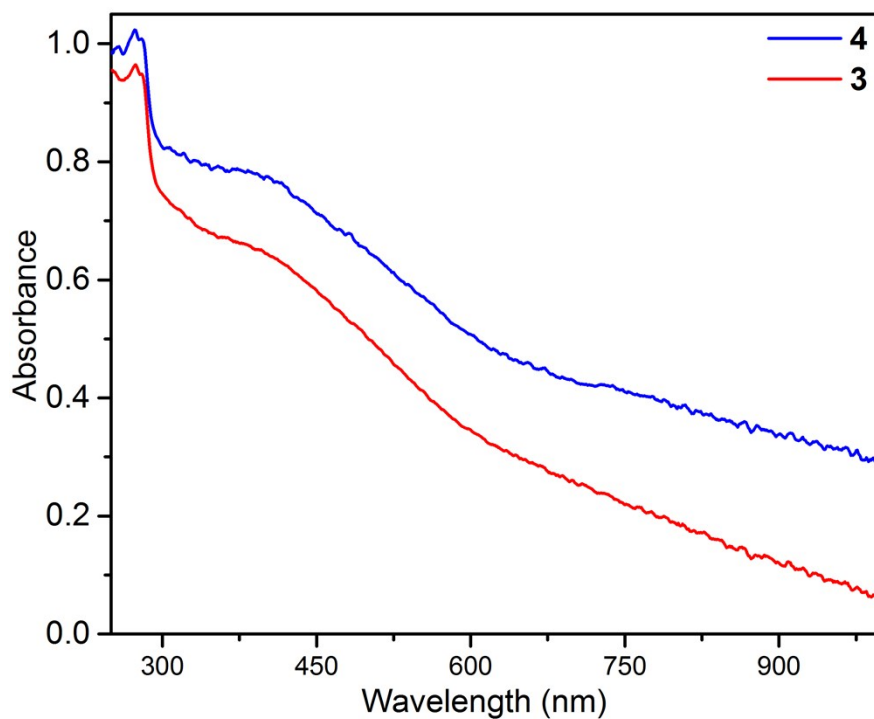


Figure S11. Absorption spectroscopic signatures for **3** and **4** as solid samples.

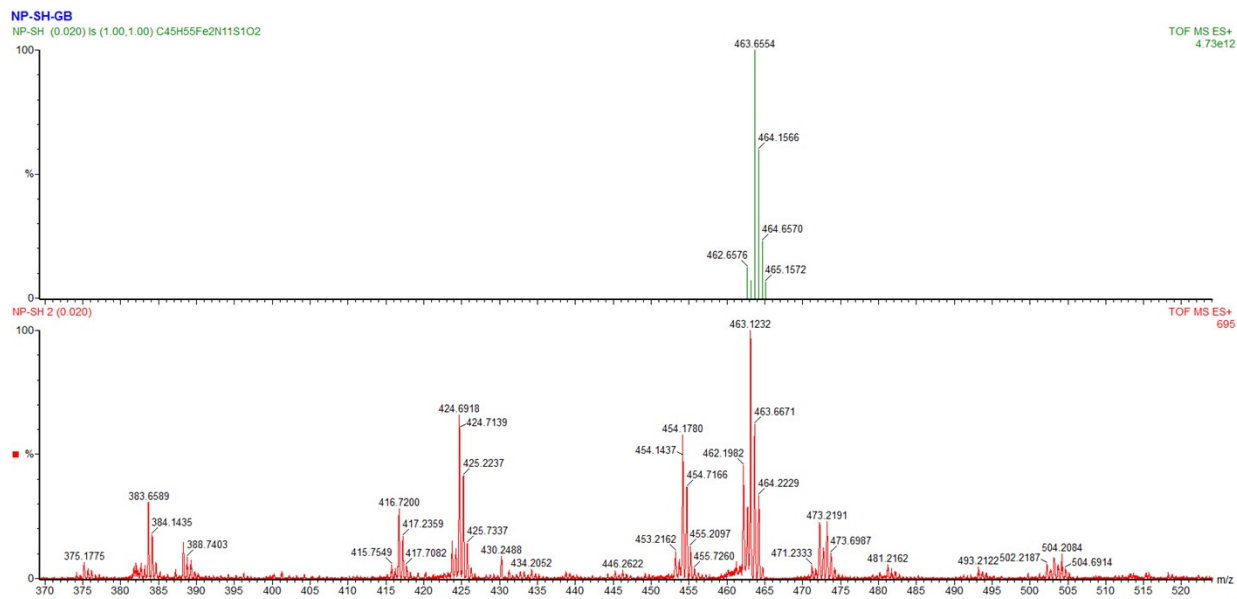


Figure S12. Mass spectrometric data for **1a** in MeCN. m/z calculated for $[\text{Fe}_2(\text{N-Et-HPTB})(\text{SH})(\text{H}_2\text{O})(\text{MeCN})]^{2+} = 463.655$ (simulated, green line), m/z observed = 463.123 (red line).

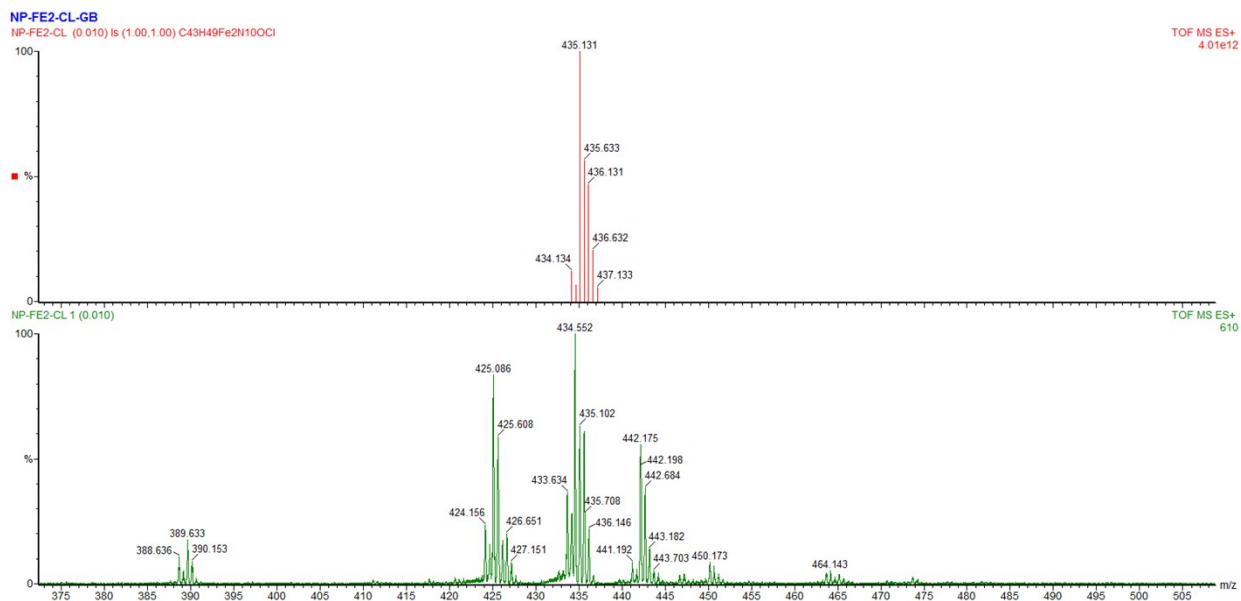


Figure S13. Mass spectrometric data for **2** in MeCN. m/z calculated for $[\text{Fe}_2(\text{N-Et-HPTB})(\text{Cl})(\text{DMF})_2]^{2+} = 435.131$ (simulated, red line), m/z observed = 434.552 (green line).

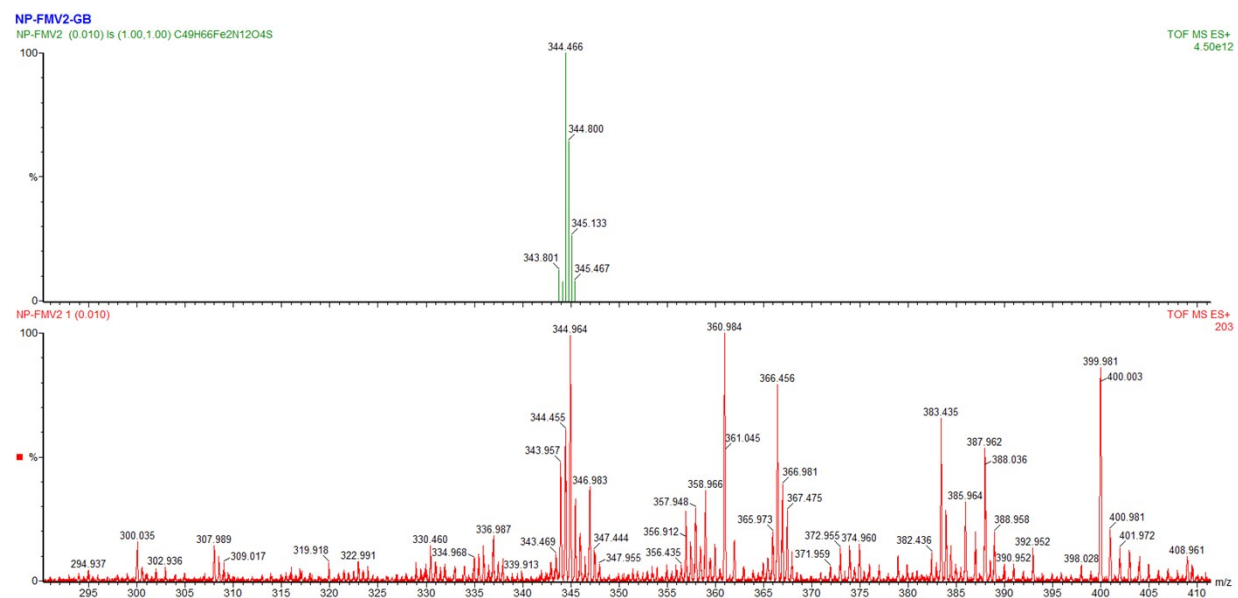


Figure S14. Mass spectrometric data for **3** in MeCN. m/z calculated for $[\text{Fe}_2(\text{N-Et-HPTB})(\text{SH})(\text{H}_2\text{O})(\text{DMF})_2]^{3+} = 344.466$ (simulated, green line), m/z observed = 344.964 (red line).

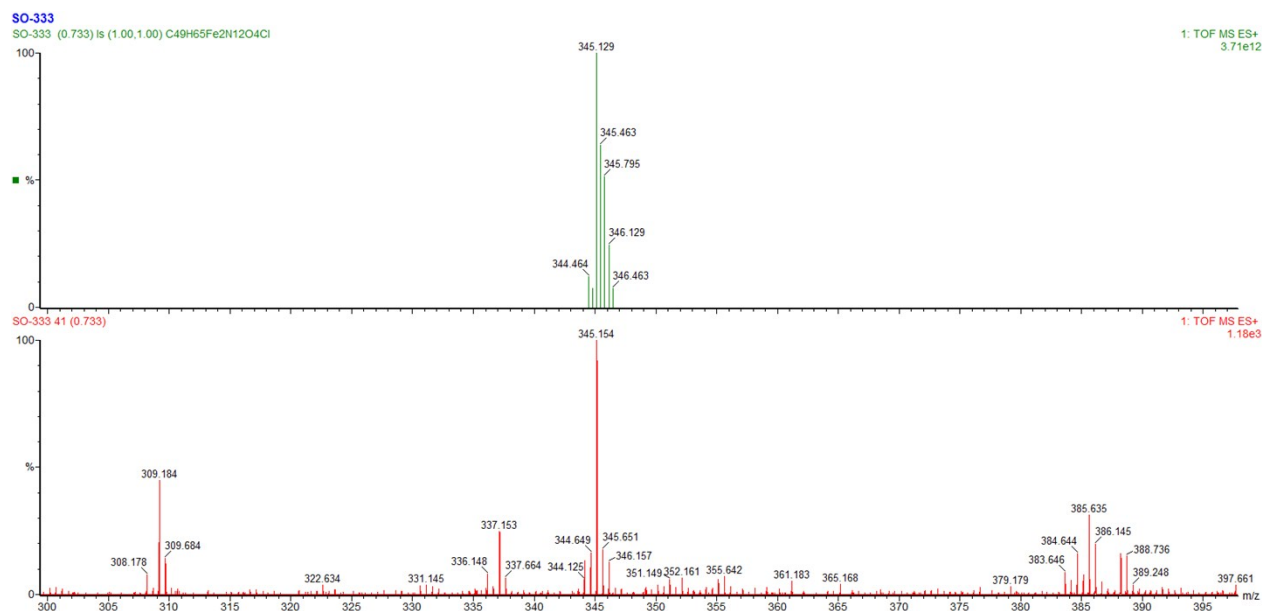


Figure S15. Mass spectrometric data for **4** in MeCN. m/z calculated for $[\text{Fe}_2(\text{N-Et-HPTB})(\text{Cl})(\text{H}_2\text{O})(\text{DMF})_2]^{3+} = 345.129$ (simulated, green line), m/z observed = 345.154 (red line).

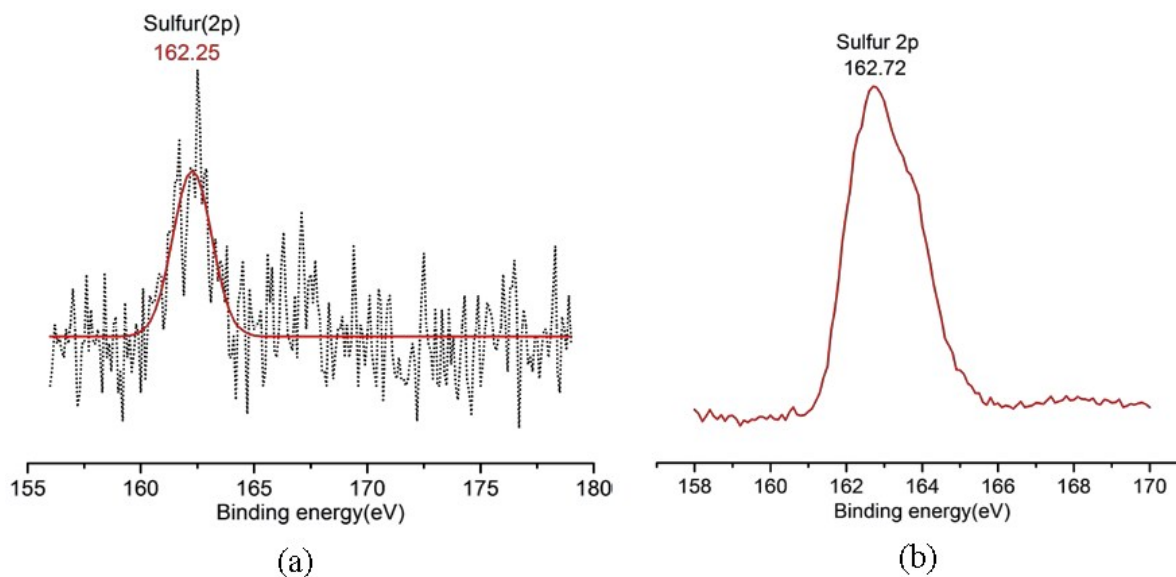


Figure S16. X-ray photoelectron spectroscopic data showing binding energy for the sulfur 2p levels of (a) **1a** and (b) **3**.

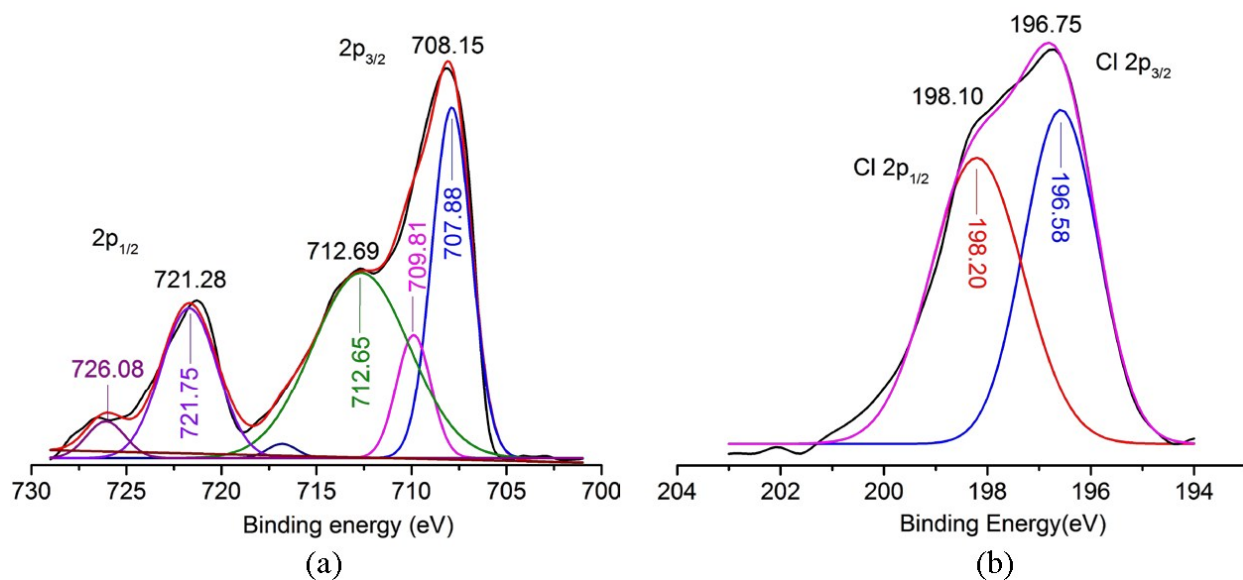


Figure S17. X-ray photoelectron spectroscopic data showing binding energy for the (a) Fe 2p levels and (b) chlorine 2p levels of **2**.

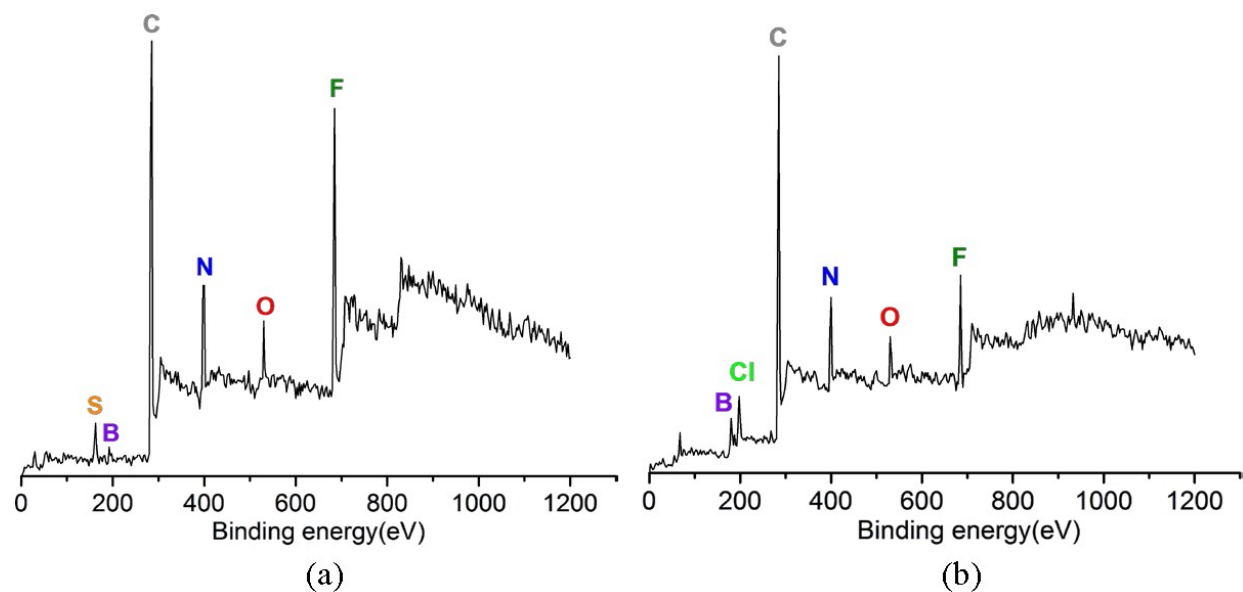


Figure S18. Full range plot of the X-ray photoelectron spectroscopic data for (a) **1a** and (b) **2**.

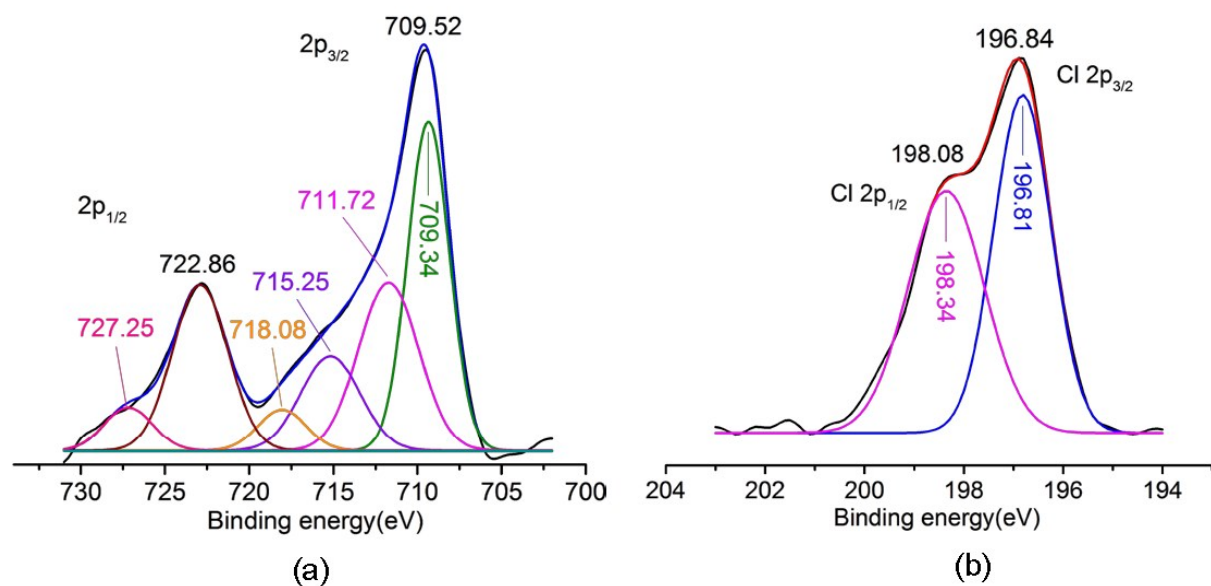


Figure S19. X-ray photoelectron spectroscopic data showing binding energy for the (a) Fe 2p levels and (b) chlorine 2p levels of **4**.

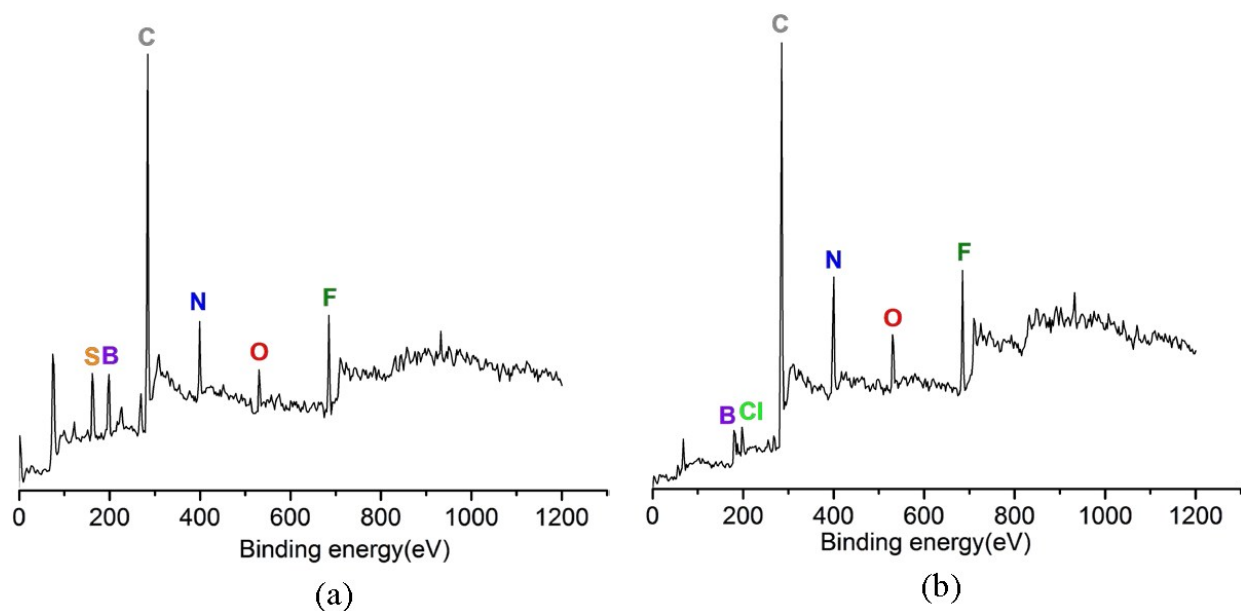


Figure S20. Full range plot of the X-ray photoelectron spectroscopic data for (a) **3** and (b) **4**.

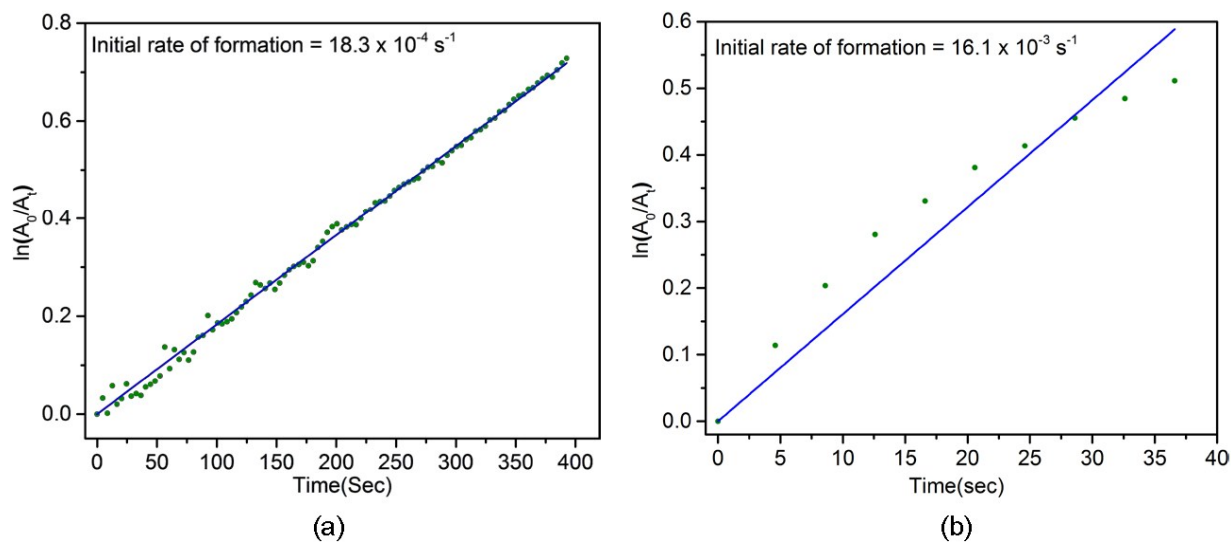


Figure S21. Kinetic plots for the initial rate of formation of (a) $1\mathbf{a}\cdot\text{O}_2$ and (b) $2\cdot\text{O}_2$ at -80°C .

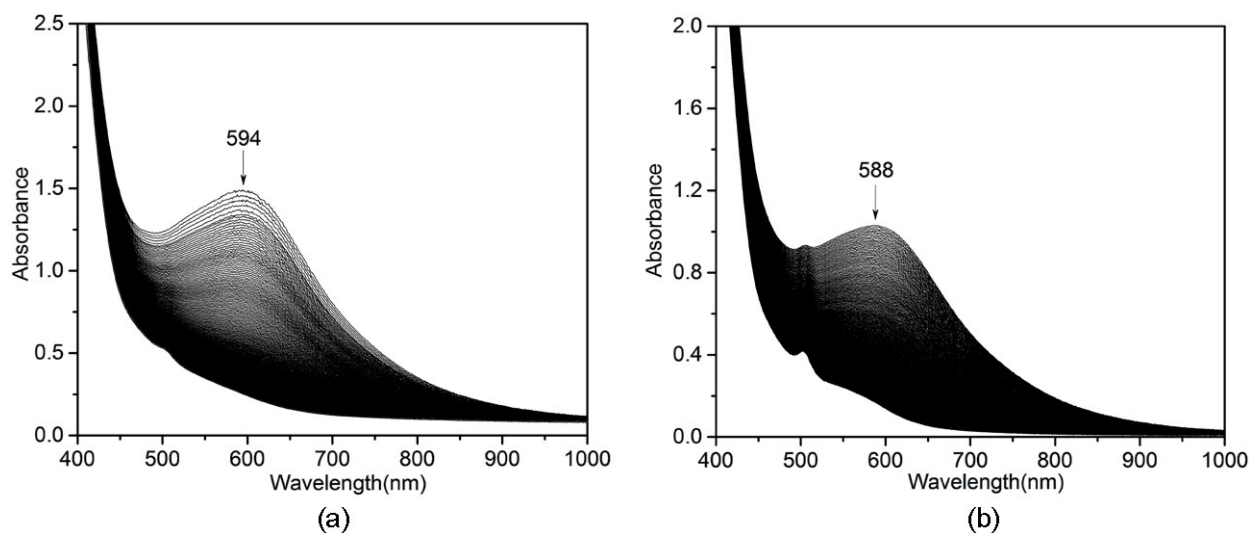
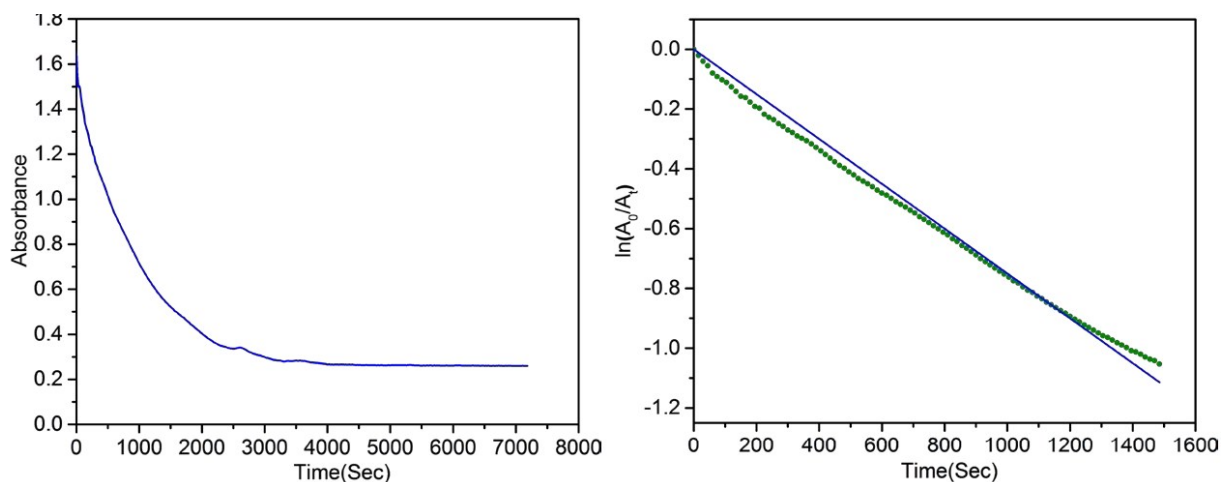
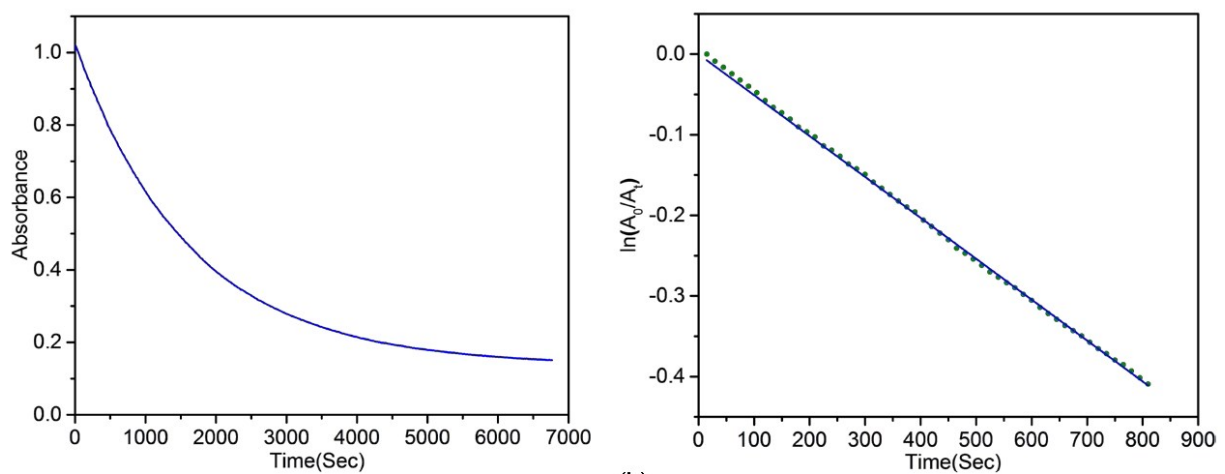


Figure S22. Absorption spectroscopic monitoring for the decomposition of (a) $1\mathbf{a}\cdot\text{O}_2$ and (b) $2\cdot\text{O}_2$ at RT. $[1\mathbf{a}] = 0.75 \text{ mM}$ in $\text{CH}_2\text{Cl}_2:\text{DMSO}$ (10:1), O_2 purged for 30 seconds, scan rate = 15 seconds/scan, total time = 120 minutes. $[2] = 0.5 \text{ mM}$ in $\text{CH}_2\text{Cl}_2:\text{DMSO}$ (10:1), O_2 purged for 10 seconds, scan rate = 15 seconds/scan, total time = 110 minutes.



(a)



(b)

Figure S23. Kinetic plots (decomposition traces and half life calculations) for the decomposition of (a) $1a \cdot O_2$ ($t_{1/2} = 15.4$ minutes) and (b) $2 \cdot O_2$ ($t_{1/2} = 22.8$ minutes) at RT. Decomposition product in each case was characterized as $[Fe_4(N-Et-HPTB)_2(\mu-O)_3(H_2O)_2](BF_4)_2$.⁴

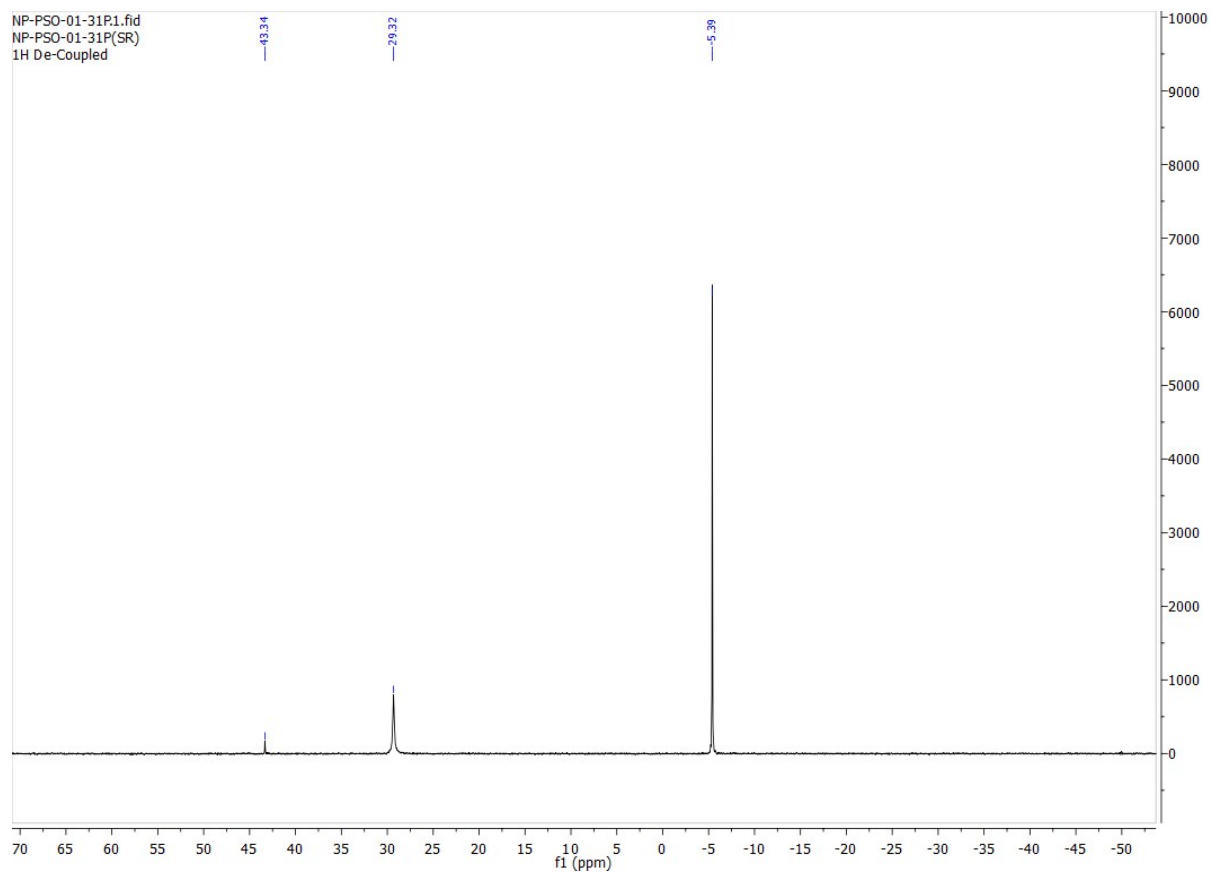


Figure S24. ^{31}P NMR spectrum for the product obtained after reaction of $\mathbf{1a}\cdot\text{O}_2$ with PPh_3 at RT showing the presence of Ph_3PS ($\delta = 43.34$ ppm) along with Ph_3PO ($\delta = 29.32$ ppm) and unreacted PPh_3 ($\delta = -5.39$ ppm).

Fe2-P-31P.1.fid
Fe2-P-31P(SR)
1H De-Coupled

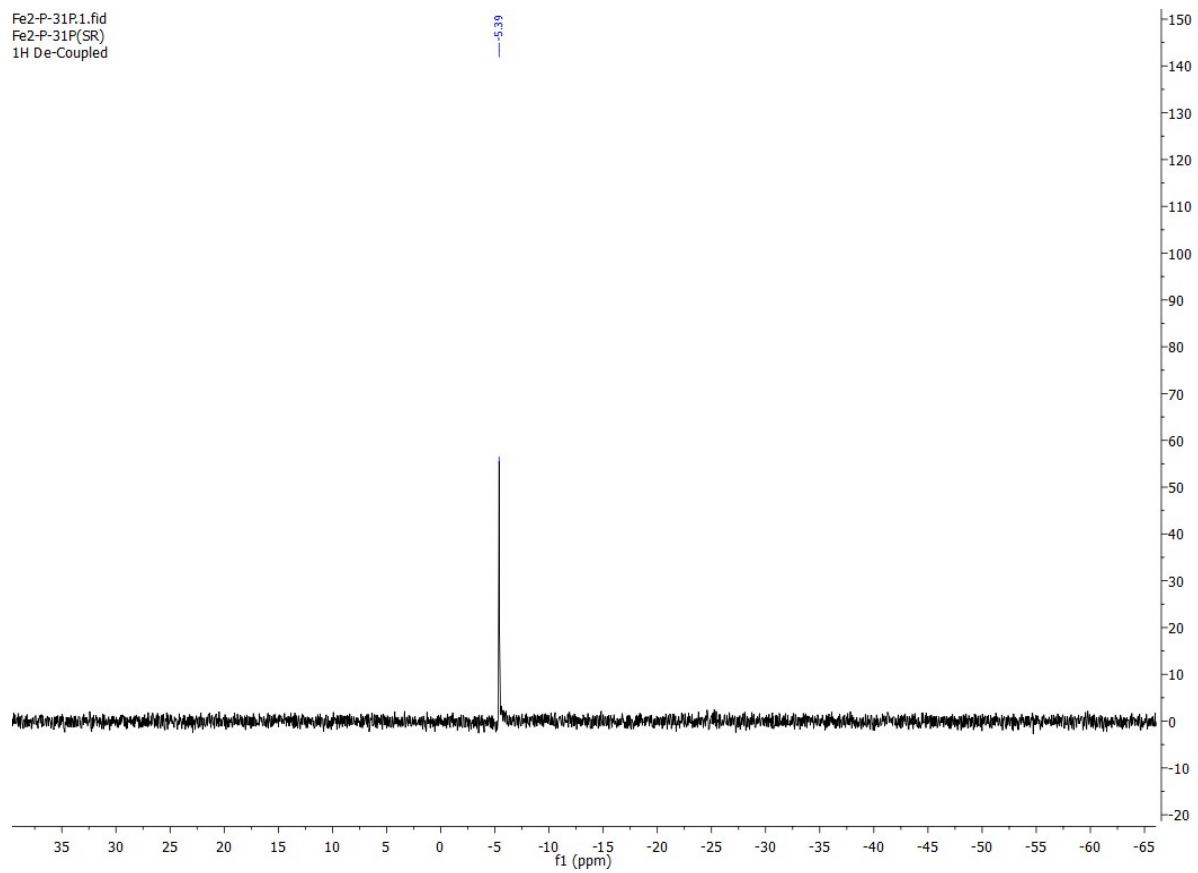


Figure S25. ^{31}P NMR spectrum for the product obtained after reaction of $\mathbf{1a}\cdot\text{O}_2$ with PPh_3 at -40°C showing the presence of only PPh_3 ($\delta = -5.39$ ppm).

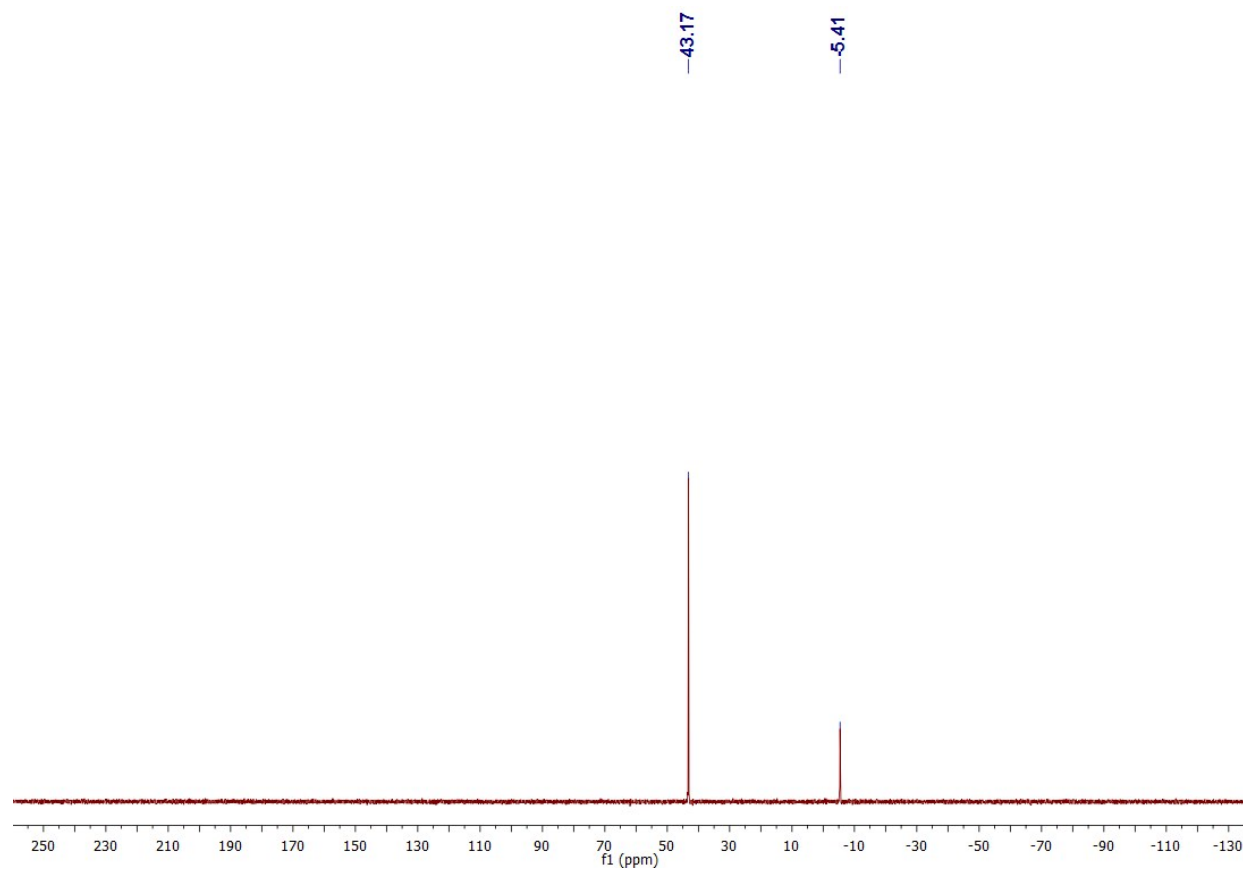


Figure S26. ^{31}P NMR spectrum for the product obtained after stirring elemental sulfur (S_8) in toluene at -40°C overnight, followed by filtration, evaporation of the filtrate and reaction of the residue with PPh_3 in CDCl_3 at RT, showing the presence of PPh_3 ($\delta = -5.41$ ppm) and Ph_3PS ($\delta = 43.17$ ppm).

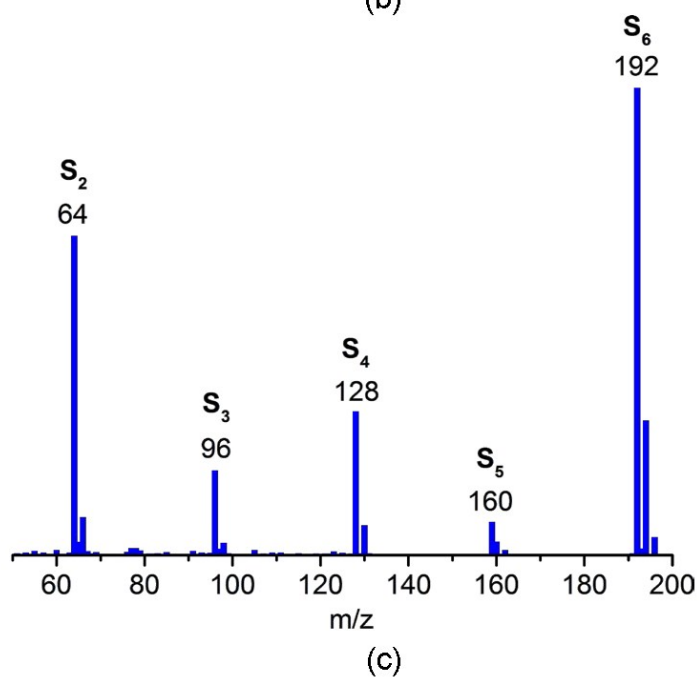
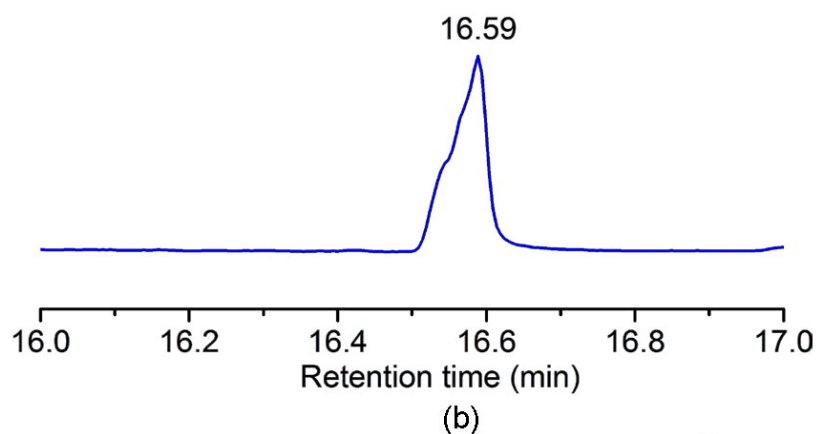
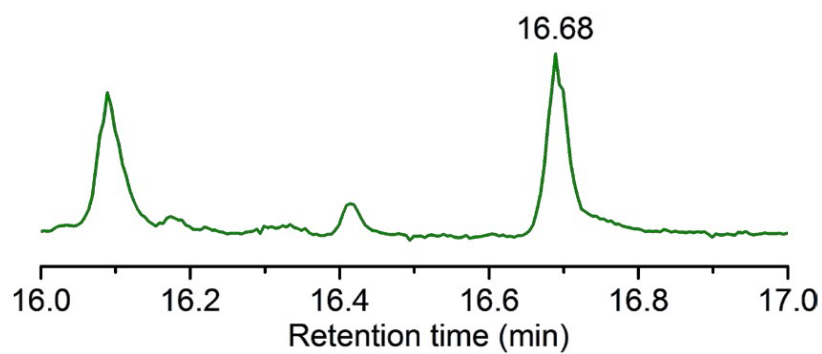


Figure S27. GC traces for (a) elemental sulfur (S_8 , 0.1 mM in CCl_4) and (b) elemental sulfur produced upon decomposition of $1\mathbf{a}\cdot\text{O}_2$ at RT. Also shown is the GCMS data for the elemental sulfur produced upon decomposition of $1\mathbf{a}\cdot\text{O}_2$ at RT (c).

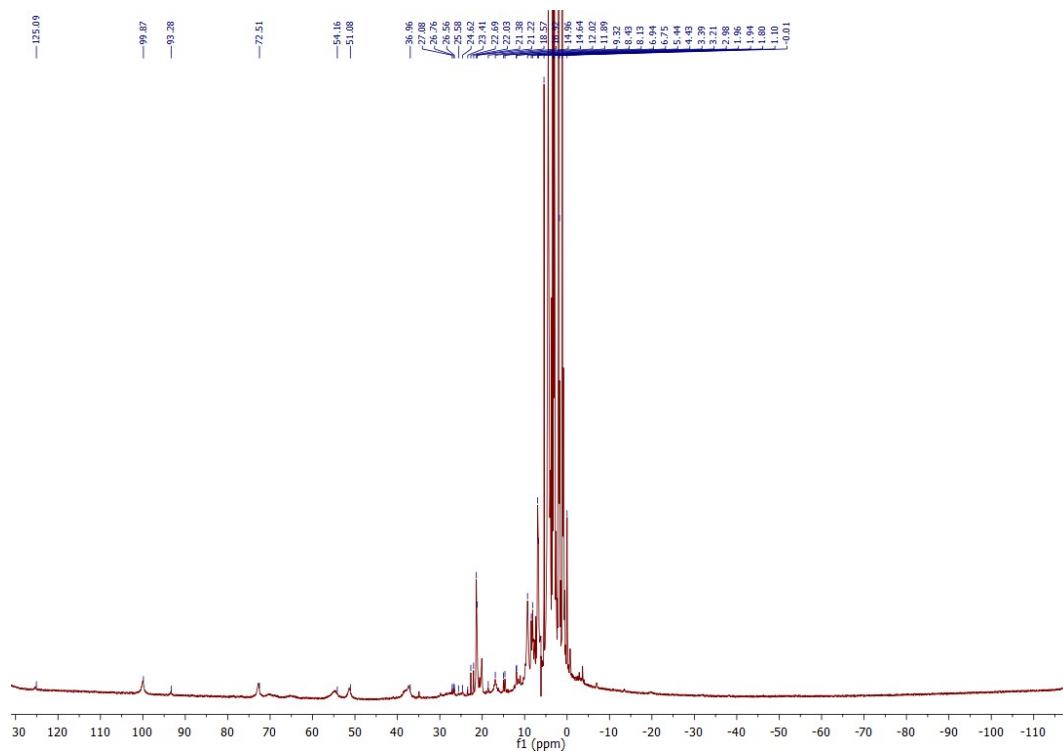


Figure S28. ^1H NMR of **1a** in CD_3CN .

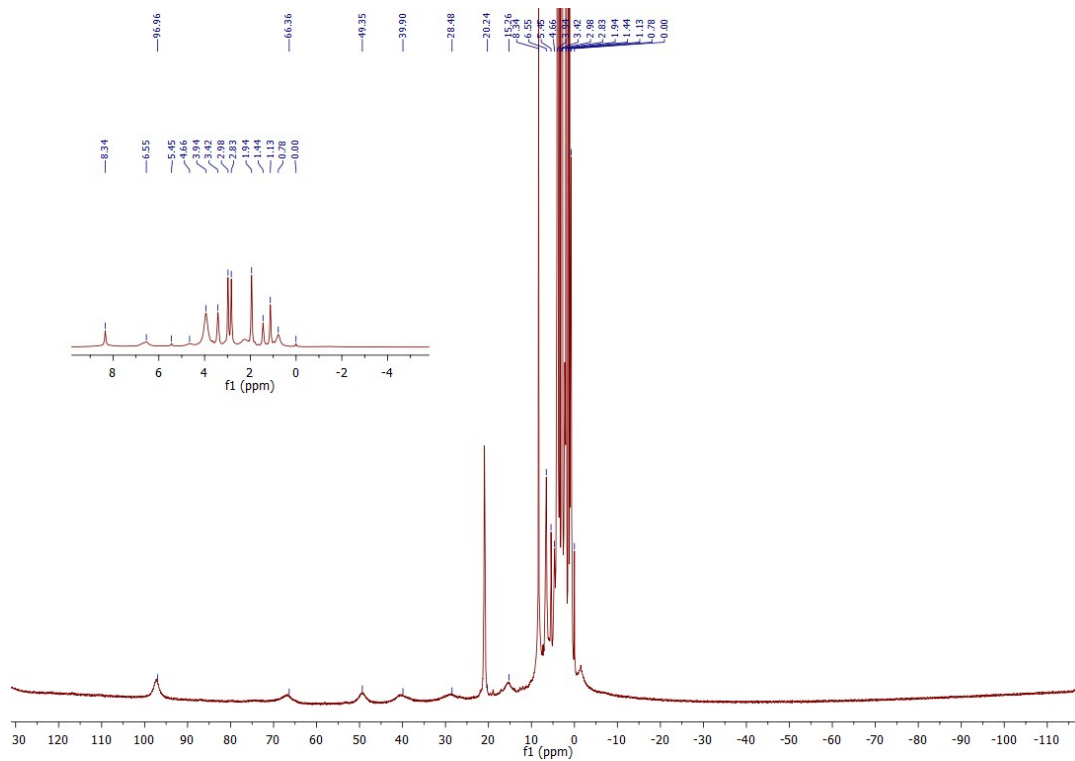


Figure S29. ^1H NMR of **2** in CD_3CN .

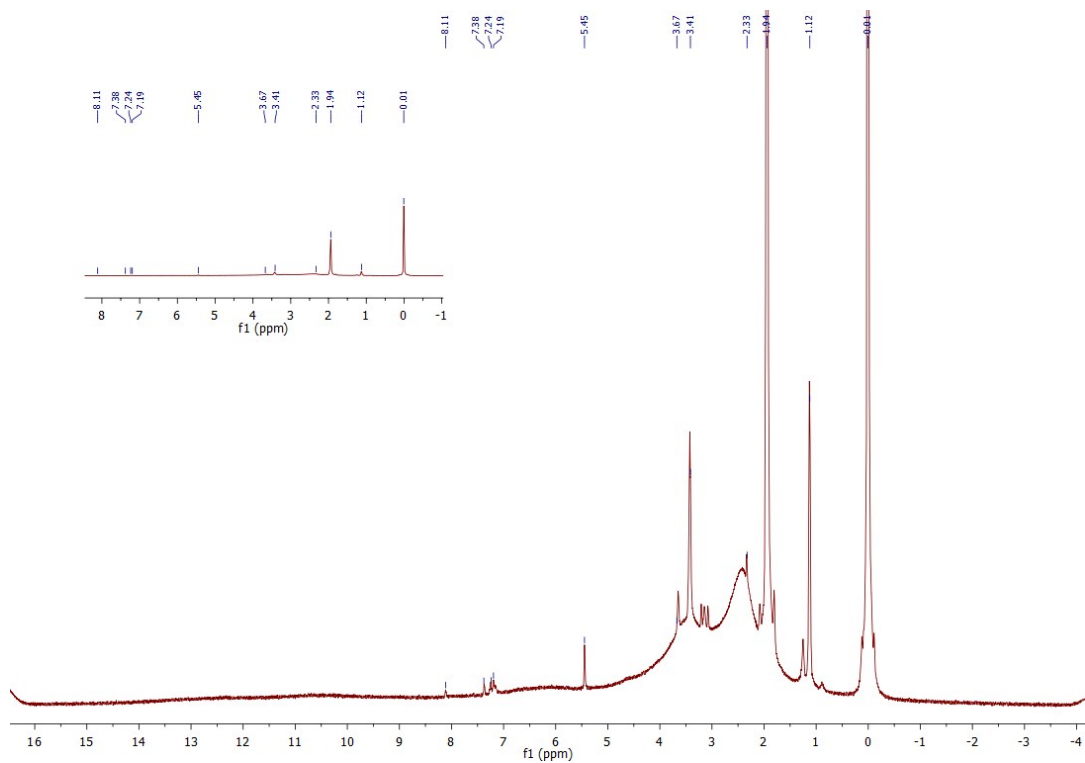


Figure S30. ^1H NMR of **3** in CD_3CN .

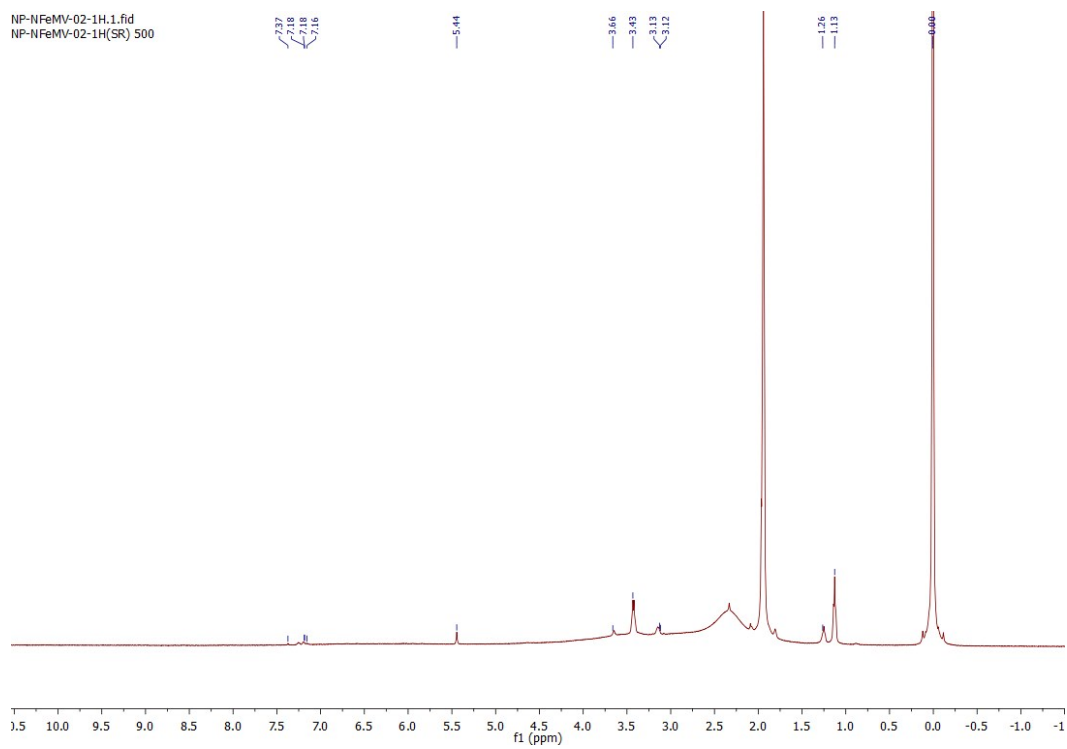


Figure S31. ^1H NMR of **4** in CD_3CN .

References.

- (1) Armarego, W. L. F.; Chai, C. L. L. *Purification of Laboratory Chemicals*; Sixth ed.; Butterworth-Heinemann, Elsevier Inc.: USA, 2009.
- (2) Pal, N.; Majumdar, A. *Inorg. Chem.* **2016**, *55*, 3181-3191.
- (3) McKee, V.; Zvagulis, M.; Dagdigian, J. V.; Patch, M. G.; Reed, C. A. *J. Am. Chem. Soc.* **1984**, *106*, 4765-4772.
- (4) Majumdar, A.; Apfel, U.-P.; Jiang, Y.; Moënne-Loccoz, P.; Lippard, S. J. *Inorg. Chem.* **2014**, *53*, 167-181.
- (5) APEX II 2009 Ed.; Bruker Analytical X-ray Systems Inc.: Madison, WI, 2009.
- (6) Spek, A. L. *J. Appl. Crystallogr.* **2003**, *36*, 7-13.
- (7) Spek, A. L. *Acta Cryst. D* **2009**, *65*, 148-155.
- (8) Sheldrick, G. M. *Acta Cryst. A* **2008**, *64*, 112-122.
- (9) Dolomanov, O. V.; Bourhis, L. J.; Gildea, R. J.; Howard, J. A. K.; Puschmann, H. *J. Appl. Crystallogr.* **2009**, *42*, 339-341.
- (10) Farrugia, L. J. *J. Appl. Crystallogr.* **1997**, *30*, 565.
- (11) Farrugia, L. J. *J. Appl. Crystallogr.* **2012**, *45*, 849-854.